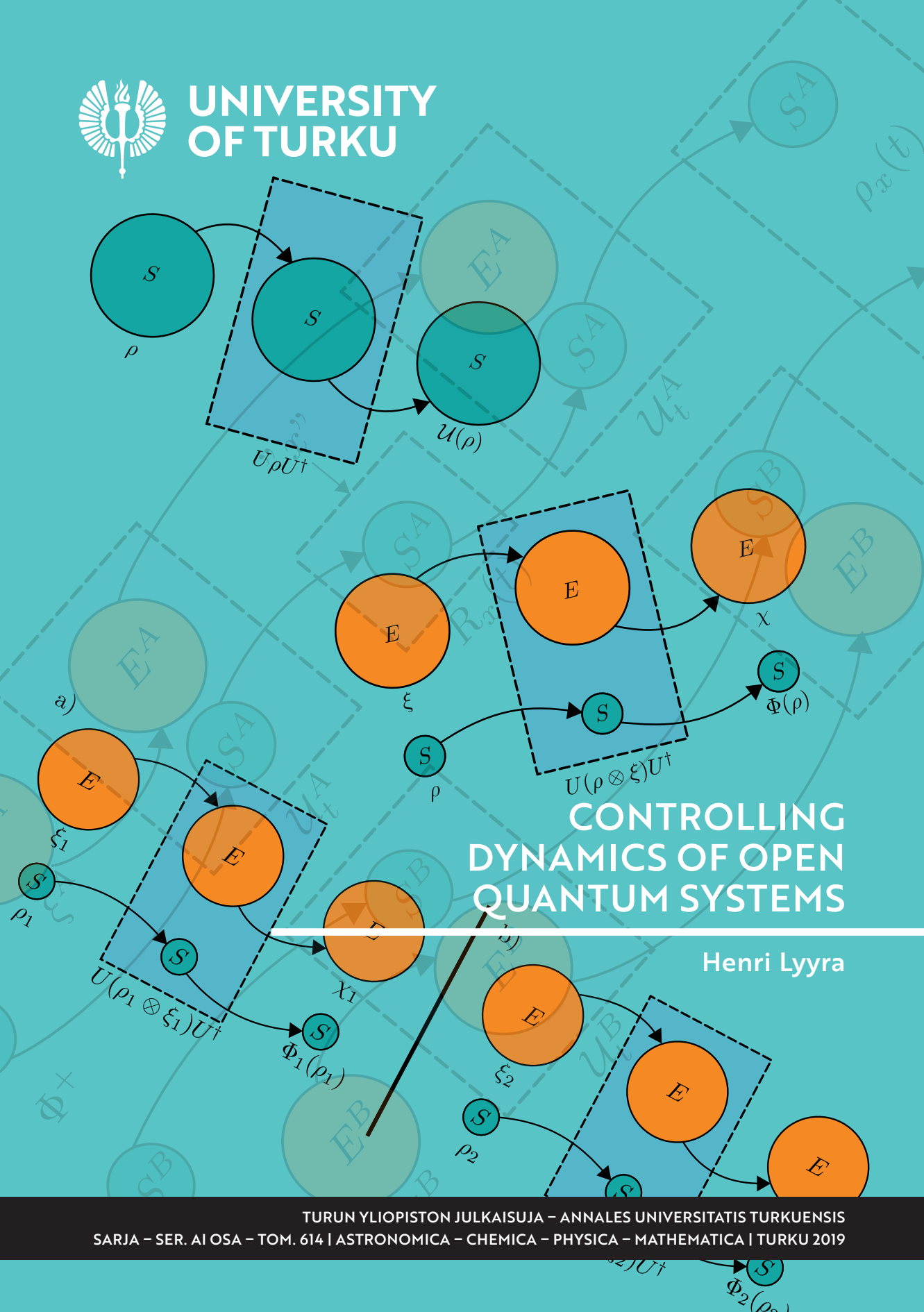
UNIVERSITY
OF TURKU
CONTROLLING
DYNAMICS OF OPEN
QUANTUM SYSTEMS
Henri Lyyra
TURUN YLIOPISTON JULKAISUJA – ANNALES UNIVERSITATIS TURKUENSIS
SARJA – SER. AI OSA – TOM. 614 | ASTRONOMICA – CHEMICA – PHYSICA – MATHEMATICA | TURKU 2019

UNIVERSITY OF TURKU

CONTROLLING DYNAMICS OF OPEN QUANTUM SYSTEMS

Henri Lyyra

TURUN YLIOPISTON JULKAISUJA – ANNALES UNIVERSITATIS TURKUENSIS
SARJA – SER. AI OSA – TOM. 614 | ASTRONOMICA – CHEMICA – PHYSICA – MATHEMATICA | TURKU 2019

University of Turku

Faculty of Science and Engineering
Department of Physics and Astronomy

Supervised by

Jyrki Piilo
Department of Physics and Astronomy
University of Turku
Finland

Sabrina Maniscalco
Department of Physics and Astronomy
University of Turku
Finland

Reviewed by

Michael J. W. Hall
Griffith University
Centre for Quantum Dynamics
Australia

Stefano Olivares
Dipartimento di Fisica
Università degli Studi di Milano
Italy

Opponent

Lorenzo Maccone
Dipartimento di Fisica
Università di Pavia
Italy

ISBN 978-951-29-7762-8 (PRINT)
ISBN 978-951-29-7763-5 (PDF)
ISSN 0082-7002 (Print)
ISSN 2343-3175 (Online)
Painosalama - Turku, Finland 2019

Acknowledgements

Despite the fact that working on a thesis is mainly lonely work, the help and support from others has been crucial in everything from studies to research - and eventually - writing of thesis. It is impossible to overstate the importance of co-workers, friends, and family.

I thank Michael J. W. Hall and Stefano Olivares for pre-examining this thesis and my opponent Lorenzo Maccone. All the work and research could not have been possible without my supervisors: Jyrki, who taught me the secrets of motorboats and put *super* in supervisor, and Sabrina, who always puts the people in our laboratory before everything.

Jose and Walter, during my time as the office boss I admired your growing passion for research and saw promising progress in the levels of nonsense too. Now, it is time for you to teach the ways of the Noisy room to Olli. As the last of the original *Noisy room bois*, I can safely leave you kids by yourselves, confident that nothing can stop you from gaining your degree. Soon, I will hopefully join the very selective bättre folk of the noisy room alumni. Talking of whom, I am grateful to Erkka for enlightening us with the endless anecdotes on Bernard Shaw's life; I want to thank Francesco for always lightening the mood with his ability to be easily impressed and find things ironic; and thank you Mikko for being the big brother I never had, guiding me and taking care of everything. Never forget Kaljaviesti 2016 – the glory shall not fade away!

Sina, I enjoyed the numerous scientific discussions. Always maintain your unmatched ability to laugh at the worst jokes – no matter how rough it gets. Thank you Teiko, for the uncountable discussions on the foundations of quantum theory and axiomatization of real numbers[1]. I am grateful to Tom for teaching me nearly everything essential about two-photon polarization experiments during my summer internship. Later, this know-how became very useful when collaborating with the Hefei group: I wish to thank Chuan-Feng, Zhao-Di, Bi-Heng, and Yong-Nan for the successful project.

[1]For brevity, we do not consider the axiomatization of real numbers in this thesis.

Every spring, I was inspired by the enthusiastic students of Quantum Mechanics I. I also had the pleasure to teach alongside T. J. Bullock, who is rightfully the leading expert on The Simpsons quotes, in my absence. Boris, Juho, and Leevi, thank you for the peer support and the comedic moments in the master students' room.

I feel sad to leave the laboratory, since I enjoyed spending time with all the people, be it a lunch, a coffee break or the Halloween movie marathon. I consider all of you my friends. To keep it short, I thank you all for the great atmosphere throughout the years. Take good care of each other.

Thank you Janne, Samuli, Tuomo, and Janne for all the unforgettable study sessions and adventures we had during our studies. Laura, thank you for the years we shared. My *brothers in iron*, both in the laboratory and out, Simo, Oskari, Juha-Pekka, Walt, Guille, Tapani, Joel, Toni, Pyry, Tuomas, Tomas, Teemu, and last but definitely most importantly Laura and Leevi: During my studies, you have helped me take care of myself, push further, and keep me sane. Thanks to all my school friends for the time we shared growing up and for keeping in touch after all these years, especially Simo, Eero, Jesse, Hennu, Juha, Pablo, Paavo, Juppe, Kalle, Niko, Pauli, Niklas, and Juuso.

Lastly, my whole family, both the sides of Lyyra and Ahola, has always been there for me and given their full support in everything I have faced. I want to especially thank Iskä, Äiti, Riina, Reeta, and Tapio-Ukki for your support and encouraging words. This thesis is dedicated to Sinikka-Mummi, who will always live on in our memories.

Contents

Abstract

Quantum mechanics has both deepened our understanding of the physical reality and allowed development of quantum technologies beating their classical counterparts in efficiency, security, and sensitivity. As a major downside, the quantum properties behind these technologies are very sensitive to the effects the system's interaction with its environment. The theory of open quantum systems describes how such interaction influences the system, and as a consequence, how the quantum features are lost, controlled, and possibly returned by manipulating the environment.

This thesis begins with a short description of the most relevant features and results of the open quantum system theory. We continue by presenting some commonly used measures to quantify the information encoded in quantum systems and the correlations between spatially or temporally separated parties. The literature review ends with discussion of non-Markovianity and memory effects which combine the fields of open quantum systems and quantum information in a natural way.

The rest of the thesis presents the main results of Publications **I** – **VII**. We study the memory effects and physicality conditions of open system dynamics described by the vast family of phase-covariant master equations. We show how the open quantum system picture can be exploited to design probing protocols to extract information without knowing how the probe and system interact. Such protocols are considered also from the point-of-view of efficiently obtaining the information required in the probing, both in theory and by experimental implementation. The experiment serves also as evidence for applicability of recently developed geometric tools to design informationally incomplete measurements for solving so-called membership problems.

We present and experimentally realize a protocol where control over intial correlations between polarization and frequency gives full freedom to implement any dephasing dynamics in the open system polarization, thus dictating how its information content changes in time. We study the

two-qubit memory effects of dephasing dynamics and compare them to the effect of such noise in the transmission efficiency in superdense coding. Optimal noise configurations in different situations are found. Finally, we characterize the families of initial states for which the decay of quantum correlations depends or does not depend on the noise location.

Tiivistelmä

Sen lisäksi, että kvanttimekaniikka on valtavasti lisännyt ymmärrystämme havaittavasta todellisuudesta, sen omituiset ilmiöt ovat myös sallineet klassisia vastineitaan tehokkaampien, turvallisempien ja hellävaraisempien kvanttiteknologioiden kehittämisen. Suurena haittapuolenaan nämä teknologiat mahdollistavat kvanttiominaisuudet ovat äärimmäisen herkkiä systeemin ja sen ympäristön väliselle vuorovaikutukselle. Avointen kvanttisysteemien teoria kuvaa, kuinka tällainen vuorovaikutus vaikuttaa systeemiin, ja tästä seuraten, kuinka kvanttiominaisuudet katoavat, miten niitä voidaan hallita – ja kuinka ne voidaan palauttaa ympäristöä muokkaamalla.

Tämä väitöskirja alkaa lyhyellä yhteenvedolla avointen kvanttisysteemien teorian tärkeimmistä ominaisuuksista ja tuloksista. Esittelemme myös joitakin yleisesti käytettyjä mittoja kvanttisysteemiin koodatun informaation ja spatiaalisesti tai ajallisesti erotettujen osapuolien välisten korrelaatioiden kuvaamisessa. Kirjallisuuskatsauksen päätteeksi käsittelemme epä-Markovisuuden ja muisti-ilmiöiden käsitteitä, jotka yhdistävät avoimet kvanttisysteemit ja kvantti-informaation luontevalla tavalla.

Väitöskirjan loppuosassa esittelemme julkaisujen **I** – **VII** tärkeimmät tulokset. Tarkastelemme laajan vaihesiirto-kovarianttien master-yhtälöiden kuvaamien dynaamisten karttojen muisti-ilmiöitä ja fysikaalisuusehtoja. Näytämme, kuinka avointen kvanttisysteemien teorian avulla voidaan kehittää epäsuoria kvanttiluotausmittausmenetelmiä, joissa luotaimen ja mitattavan systeemin välistä vuorovaikutusta ei tunneta. Tarkastelemme näitä menetelmiä myös mittauksessa tarvittavan informaation saamisen näkökulmasta sekä teoreettisesti että kokeellisesti. Kokeemme osoittaa myös, kuinka vastikään kehitetyt geometriset työkalut kvanttitilojen jäsenyysongelmia ratkaisevien informatiivisesti epätäydellisten mittausten suunnitteluun toimivat myös käytännössä.

Esittelemme ja kokeellisesti toteutamme menetelmän, jossa polarisaation ja taajuuden alkukorrelaatioita hallitsemalla voidaan täydellisesti hallita sitä, miten polarisaatio avoimena systeeminä muuttuu dephasing-melun

vaikutuksesta ajassa. Täten myös polarisaatioon koodatun informaation määrää hallitaan. Tarkastelemme kahden kubitin muisti-ilmiöitä dephasing-melussa ja vertaamme niitä näiden melujen vaikutuksiin superdense coding -menetelmän lähetystehokkuuteen. Selvitämme myös suotuisimmat melukonfiguraatiot eri tilanteissa. Lopulta luokittelemme ne alkutilajoukot, joiden kvanttikorrelaatioiden katoaminen riippuu tai ei riipu melun sijainnista.

List of papers

This thesis consists of a review of the subject and the following original research articles:

I **Non-Markovian dynamics in two-qubit dephasing channels with an application to superdense coding**,
A. Karlsson, *H. Lyyra*, E.-M. Laine, S. Maniscalco, J. Piilo, Phys. Rev. A **93**, 032135 (2016)

II **Complete positivity, finite-temperature effects, and additivity of noise for time-local qubit dynamics**,
J. Lankinen, *H. Lyyra*, B. Sokolov, J. Teittinen, B. Ziaei, S. Maniscalco, Phys. Rev. A **93**, 052103 (2016)

III **Fidelity of dynamical maps**,
M. Tukiainen, *H. Lyyra*, G. Sarbicki, S. Maniscalco, Phys. Rev. A **95**, 052102 (2017)

IV **Symmetry in the open-system dynamics of quantum correlations**,
H. Lyyra, G. Karpat, C.-F. Li, G.-C. Guo, J. Piilo, S. Maniscalco, Sci. Rep. **7**, 8367 (2017)

V **Revealing memory effects in phase-covariant quantum master equations**,
J. Teittinen, *H. Lyyra*, B. Sokolov, S. Maniscalco, New J. Phys. **20**, 073012 (2018)

VI **Experimental implementation of fully controlled dephasing dynamics and synthetic spectral densities**,
Z.-D. Liu, *H. Lyyra*, Y.-N. Sun, B.-H. Liu, C.-F. Li, G.-C. Guo, S. Maniscalco, J. Piilo, Nature Communications **9**, 3453 (2018)

VII **Obtaining conclusive information from incomplete experimental quantum tomography**,
H. Lyyra, T. Kuusela, T. Heinosaari, Phys. Rev. A **99**, 042335 (2019)

Chapter 1

Introduction

Since its earliest discoveries, quantum mechanics has revolutionized the way we understand Nature: A particle can be prepared in superpositions, allowing it to counter-intuitively interfere with itself [1, 2]. There exist pairs of observables which are fundamentally incompatible [3, 4] and any non-trivial measurement changes the system's state [5–7] – if the path of the particle can be observed in any way, the interference pattern disappears, and if the path information is erased the interference reappears [8–10]. In addition, the total state can never be obtained by any measurement on a single copy of the system, nor can an unknown state be perfectly copied [11, 12]. Still, the unknown state can be perfectly copied and encoded into another system, no matter how far, by quantum teleportation once the original state has been fully destroyed [13]. The superposition enables a "super-classical" type of correlation between distant particles, namely entanglement [14–16]. Bipartite states whose subsystems are entangled can be used to show that the seemingly intuitive requirement of local realism for physical theory is violated by quantum mechanics [17, 18]. As the experimental know-how improved, these bizarre phenomena have passed thorough testing time after time [19–21].

As our understanding of the quantum world increased, exploiting these quantum features in new technologies began. Different quantum communication protocols have been developed, making communication safer [22, 23] or more efficient [24] than classical and enabling teleportation of unknown quantum states [13]. Quantum algorithms outperforming their classical counterparts have been proposed [25–28] and experimentally implemented [29–31]. Nowadays, there are even satellites on Earth's orbit for quantum key distribution, quantum teleportation and distribution of entangled pairs of qubits [20, 32], and small-scale quantum computers are already freely in

the use of anyone [33, 34].

Despite the apparent and fast progress, quantum technologies face one fundamental problem: as the number of qubits increases, the device becomes more prone to lose its quantum properties as it interacts with the environment [35, 36]. Generally, we say that a system is open if it interacts with some other system. Since any realistic system is open, the field of open quantum systems has attracted a lot of attention [37–40]. Understanding how open system dynamics influences the system has allowed developing solutions to the problems it causes: As the information carrier experiences open system dynamics, it loses information to the environment. Because the system cannot be perfectly isolated from the environment, reservoir engineering techniques have been studied to minimize the detrimental effects [36, 41]. Recently, quantifying information back flow and non-Markovian memory effects has been an active field of research and multiple different characterizations and measures of quantum non-Markovianity have been proposed and compared extensively [42–50]. Non-Markovianity has been shown to improve experimental implementation of noisy superdense coding [51] and the Deutsch-Jozsa algorithm [52].

Even though environment-induced open system dynamics has harmful effects on the information carriers, it can be exploited to achieve multiple tasks: Closely related to reservoir engineering, in processor based quantum computing different gates can be implemented on the open system information carriers by carefully preparing the initial state of the environment [53]. As simulating complex quantum systems on classical computers is very demanding, using open quantum systems as quantum simulators has been studied [54–57]. Direct measurements on the quantum systems, acting as information carriers, influence their states, which leads to loss of useful quantum properties such as entanglement and quantum coherence. Even worse, sometimes direct measurements destroy the whole quantum system. A less invasive way of measuring a quantum system is by means of an expendable quantum probe interacting with the system. The system acts as an environment for the probe and thus induces open system dynamics. Some properties of the system can then be mapped into the dynamics of the probe. Via measuring the evolved probe, one can therefore indirectly infer information on the system, without directly influencing it. Recently, multiple quantum probing protocols have been proposed [58–63] and some of them even exploit non-Markovianity of the dynamics [60].

In this thesis, we consider the effects of open quantum system dynamics

in the context of information theory. We begin with Chapter 2 by recalling the basic definitions and concepts of Hilbert space quantum mechanics and presenting some of the main results in open quantum system theory. In chapter 3, we discuss some commonly used information and correlation measures. We also present some of the proposed definitions of quantum Markovianity and different memory effects based on the information measures.

Chapters 4 – 6 are dedicated to the main results of the thesis, reported in Publications **I** – **VII**. In Chapter 4, we concentrate on phase-covariant qubit master equations and discuss Publications **II** and **V**. Phase-covariant qubit dynamics covers a plethora of dynamical maps, both unital and non-unital, and includes all of the explicitly studied dynamics in the rest of the thesis. First, we solve the conditions for the map to be completely positive and trace preserving, which correspond to physicality of open system dynamics in the absence of initial system–environment correlations. Then, we solve and compare the conditions for different memory effects to occur.

We begin Chapter 5 with results of Publication **III**. We study some implications of the similarity of initial environment states, opening new possibilities in quantum probing and leading to some restrictions in reservoir engineering. Under the commonly used assumption of initially uncorrelated system and environment, we derive an inequality between the similarity of initial state pairs of the environment and the system, and the similarity of the pair of evolved open system states. So far, quantum probing protocols have relied on knowledge of the interaction between the probe system and its environment. We show how our inequality serves as a toolbox for constructing quantum probing protocols which can be employed in total ignorance of the interaction. We also point out the restrictions imposed by our inequality to pure dephasing with unknown time dependence.

Chapter 5 continues with the results of Publication **VII**. We construct and experimentally implement an informationally incomplete measurement which can be used to obtain the required measurement data in our proposed probing protocols. At the same time, our experiment proves that the recently developed geometric framework of [64] can be used to construct realistic and implementable informationally incomplete measurements which solve membership problems of the state space.

We end Chapter 5 by discussing the results of Publication **VI**, where we go beyond the restrictions of initially uncorrelated system–environment state. Recently, limited freedom to prepare the initial state of the envi-

ronment has been shown to allow for controlled transition between Markovian and non-Markovian dephasing dynamics of open system polarization qubit [65]. We show how full control of the initial frequency state and polarization–frequency correlations lets us implement any pure dephasing dynamics of the polarization state. Previously, initial system–environment correlations have been shown to relax the physicality requirement of complete positivity [66] and violation of positivity has been used to construct a witness of initial correlations [67]. We show how precise control of initial correlations permits to engineer dynamics manifesting non-positive behavior. The results are experimentally realized and the measurement results are discussed.

In the beginning of Chapter 6, we summarize the results of Publication **I**. We consider two polarization qubits experiencing pure dephasing dynamics caused by interactions with their uncorrelated frequency environments. First we compare two memory-effect-based definitions of non-Markovinanity with the increases of transmission efficiency in noisy superdense coding. Then we concentrate on noisy superdense coding and show which choices maximize the mutual information between the sender and recipient, or the temporal increase of the mutual information. We end Chapter 6 with Publication **IV** by studying the decay of entanglement and non-locality of two-qubit states. We concentrate on the so-called X states and find the families of initial states whose correlation-decay under depolarizing and amplitude damping dynamics depends (or does not depend) on the location of the noise. We compare these families corresponding to different dynamics and see whether the location-dependence of different correlations shows any hierarchy.

In Chapter 7, we conclude by discussing the main results of the thesis and potential future research questions.

Chapter 2

Open Quantum Systems

2.1 Basic elements of quantum theory

In empirical theories, the system S is characterized by a set of preparations Π by which S can be prepared. Once the system has been prepared, information about S can be extracted by performing a measurement on it and registering the measurement outcome. Let $\pi \in \Pi$, be a possible preparation and, Σ be the set of possible measurements on S. Let $X = \{x_1, x_2, \ldots x_n\}$ be the set of possible outcomes in measurement $\sigma \in \Sigma$. The experiment, defined by the preparation, measurement, and the registered outcomes, is meaningful only if the distribution of the registered outcomes depends on the preparation: the preparation π and measurement σ should produce the probability $p_\pi^\sigma(x_i)$ of each outcome x_i so that when the experiment is repeated for $N >> 1$ identical copies of the same preparation, the relative frequency $\#(x_i)/N$ approaches $p_\pi^\sigma(x_i)$ [68].

In probabilistic theories, such as quantum mechanics, statistically indistinguishable preparations, and measurements, are identified with each other into equivalence classes. The equivalence classes of preparations are called states of S, whereas the equivalence classes of measurements are called the physical observables of S. In this thesis, we concentrate on the Hilbert space representation of quantum mechanics. For brevity, we do not consider the axiomatic derivation of Hilbert space structure and refer the reader to [69, 70].

In Hilbert space quantum mechanics, the system S is given a separable Hilbert space $\mathcal{H}^S$ with dimension d^S, meaning an inner product space of d^S dimensional complex vectors which is complete w.r.t. the norm induced by the inner product. The state space of S is $\mathcal{S}(\mathcal{H}^S) = \{\rho \in \mathcal{L}(\mathcal{H}^S) | \mathrm{tr}[\rho] = 1, \rho \geq \mathcal{O}\}$, where $\mathcal{L}(\mathcal{H}^S)$ is the set of linear operators acting on $\mathcal{H}^S$. Here

$\mathrm{tr}[A] := \sum_{i=1}^{d^S} \langle \phi_i | A | \phi_i \rangle$, where $\{\phi_i\}_{i=1}^{d^S}$ is any orthonormal basis of $\mathcal{H}^S$, is called the *trace* of operator A and we say that $A \geq \mathcal{O}$, or equivalently, A is a *positive operator* if and only if $\langle \phi | A | \phi \rangle \geq 0 \, \forall \, \phi \in \mathcal{H}^S$. In what follows, we omit the labeling superscript of the system where it is obvious.

Pure states are the elements of $\mathcal{S}(\mathcal{H})$ which cannot be written as convex combination of any other states ρ_1, $\rho_2 \in \mathcal{S}(\mathcal{H})$ as $\rho = p\,\rho_1 + (1-p)\rho_2$, for $\rho_1 \neq \rho_2$, and $p \in (0,1)$. Any pure state ρ can be represented by a vector $\phi_\rho \in \mathcal{H}$, such that $\rho = |\phi_\rho\rangle\langle\phi_\rho|$, and $\langle\, \phi_\rho \,|\, \phi_\rho \,\rangle = 1$. If state ρ is not pure, we say that it is *mixed*. For every operator ρ corresponding to qubit state, a state in the two-dimensional Hilbert space, there exists a unique *Bloch vector* $\mathbf{r} \in \mathbb{R}^3$ such that $\rho = \frac{1}{2}(\mathbb{1} + r_1\sigma_1 + r_2\sigma_2 + r_3\sigma_3)$. Here $\mathbb{1}$ is the identity operator, and σ_1, σ_2, and σ_3 are the so-called Pauli operators. A qubit state is pure if and only if the Euclidean norm of its Bloch vector is one and mixed if the norm is less than one. The points of the unit radius sphere are one-to-one with the set of qubit states and it is commonly known as the *Bloch sphere*.

Systems A and B can be combined into a bipartite system AB by forming their combined Hilbert space as $\mathcal{H}^{AB} := \mathcal{H}^A \otimes \mathcal{H}^B$, where $\otimes$ denotes tensor product. By combining more systems in the same way, more complex multi-partite systems can be formed. The subsystems of AB are completely uncorrelated if the total state can be written as $\rho^{AB} = \rho^A \otimes \rho^B$, which is a *factorized state*. Factorized states are a subset of *separable states*, which can be written as convex combinations of $\rho_i^A \otimes \rho_i^B \in \mathcal{S}(\mathcal{H}^{AB})$ as $\sum_i p_i \, \rho_i^A \otimes \rho_i^B$, $\sum_i p_i = 1$, $p_i \in [0,1] \, \forall \, i$. Unfactorized separable states manifest some correlations but only the subsystems of unseparable states, known as *entangled states*, share a stronger type of correlation, namely *entanglement* [12]. Entanglement is such a peculiar property that Schrödinger himself singled it out as "the characteristic trait of quantum mechanics" [14].

Measurements in quantum mechanics are described by *positive operator valued measures* (POVM). POVM E assigns to each measurement outcome e_i a positive operator $E_i \in \mathcal{L}(\mathcal{H})$, where the operators E_i form a complete set, $\sum_i E_i = \mathbb{1}$ [1]. If the system is prepared in state ρ, the probability of outcome e_i can be obtained as $p_\rho^E(e_i) = \mathrm{tr}[E_i\rho]$. Two states, ρ_1 and ρ_2 are distinguished from each other with E if and only if the measurement out-

[1] Since any realistically implementable measurement cannot register infinitely many outcomes, we restrict to measurements with discrete outcomes.

come probabilities $p^E_{\rho_1}(e_i)$ and $p^E_{\rho_2}(e_i)$ are different for at least one i. More formally, there is at least one i such that $\mathrm{tr}[E_i\rho_1] \neq \mathrm{tr}[E_i\rho_2]$, or equivalently $\mathrm{tr}[E_i(\rho_1 - \rho_2)] \neq 0$. From this follows that E can distinguish any pair of states if and only if there does not exist a pair ρ_1, $\rho_2 \in \mathcal{S}(\mathcal{H})$ such that $\rho_1 \neq \rho_2$ and $\mathrm{tr}[E_i(\rho_1 - \rho_2)] = 0 \,\forall\, i$. Such POVM's are called *informationally complete* (or tomographically complete), and since they can distinguish any state from others, they can be used to perform state tomography to construct the whole state of the system. If E is not informationally complete, we say that it is *informationally incomplete* [12].

2.2 Evolution of a quantum system

The only natural requirements for a dynamical map Φ_t, describing the system's time evolution, are convex-linearity $\Phi_t(p\rho + (1-p)\sigma) = p\Phi_t(\rho) + (1-p)\Phi_t(\sigma)$ and physicality [2]. The physicality means, that for any initial state $\rho(0) \in \mathcal{S}(\mathcal{H})$ the evolved state $\Phi_t(\rho(0)) = \rho(t)$ has to be a state at all times $t \geq 0$. More formally, the dynamics has to be *trace preserving* (TP), $\mathrm{tr}[\Phi_t(A)] = \mathrm{tr}[A] \;\forall\, A \in \mathcal{L}(\mathcal{H})$, and Φ_t has to be a *positive map*, meaning $\Phi_t(A) \geq \mathcal{O} \;\forall\, A \geq \mathcal{O}$ [12].

In this chapter, we study the quantum systems' dynamics in two different cases, namely closed system dynamics and open system dynamics.

2.2.1 Closed systems

We call a quantum system *closed* if it does not interact with any other system. Dynamics of a pure state $\psi(0) \in \mathcal{S}(\mathcal{H})$ of a closed system is ruled by the Schrödinger equation:

$$i\hbar \frac{\mathrm{d}}{\mathrm{d}t}|\psi(t)\rangle = H(t)|\psi(t)\rangle, \tag{2.1}$$

where $H(t)$ is the Hermitian Hamiltonian operator and $\hbar$ is the Planck constant divided by 2π. The dynamics of the system state can be solved from Eq. (2.1) as:

$$|\psi(t)\rangle = e^{-i\hbar \int_0^t H(t')dt'}|\psi(0)\rangle =: U(t)|\psi(0)\rangle \tag{2.2}$$

[2] We note that if an open quantum system is initially correlated with its environment, a dynamical map cannot be written and we refer to the evolution just as dynamics.

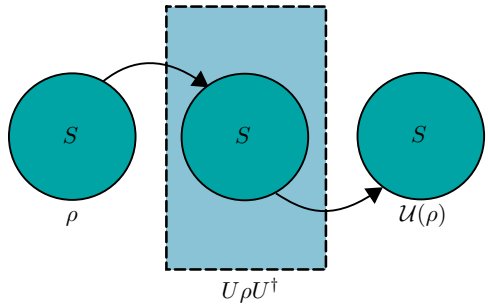

Figure 2.1: Dynamics of the closed system S.

Since $H(t)$ is Hermitian, $U(t)$ is always unitary, meaning $U(t)^\dagger U(t) = U(t)U(t)^\dagger = \mathbb{1}\,\forall\, t \geq 0$.

For mixed initial states $\rho = \sum_i p_i |\phi_{\rho_i}\rangle\langle\phi_{\rho_i}|$, the time evolution of each ensemble member state vector $|\phi_{\rho_i}(0)\rangle$ is described by the Schrödinger equation and thus can be written in the form of Eq. (2.2). The evolution of the entire ensemble, defining the mixed state, becomes

$$\rho(t) := \sum_i p_i\, U(t)|\phi_{\rho_i}(0)\rangle\langle\phi_{\rho_i}(0)|U(t)^\dagger = U(t)\rho(0)U(t)^\dagger\,, \tag{2.3}$$

so the dynamics of any closed system is described by unitary transformation, as in Fig. 2.1.

Now, using Eq. (2.2) in the time derivative of Eq. (2.3) gives us

$$\begin{aligned} \frac{\mathrm{d}}{\mathrm{d}t}\rho(t) &= -\frac{i}{\hbar}H(t)U(t)\rho(0)U(t)^\dagger + \frac{i}{\hbar}U(t)\rho(0)U(t)^\dagger H(t) \\ &= -\frac{i}{\hbar}[H(t), \rho(t)], \end{aligned} \tag{2.4}$$

where $[X, Y] := XY - YX$ is the commutator of operators X and Y [37]. We conclude by noting that unitarity of $U(t)$ and the cyclicity of trace operation guarantees that dynamical map of closed system dynamics is always positive and TP.

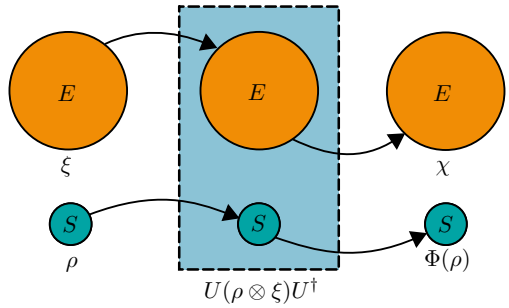

Figure 2.2: Illustration of open system S interacting with its environment E. The combination SE forms a closed system whose dynamics is governed by the unitary operator U.

2.2.2 Open systems

Unlike closed systems, *open systems* interact with some other system which we call the *environment* E of the system S, as illustrated in Fig. 2.2. In reality, no system can be perfectly isolated from the others and the only closed system is the entire universe. Thus, in practice we always do experiments and build devices with open systems. For this reason, understanding how open systems evolve during time is crucially important. The open system S can be considered as a subsystem of the larger closed system SE which is formed by coupling S and E. When studying the dynamics of S we are not usually interested in how E evolves. As we will see, by coupling S and E the states of S and E can become entangled during the total system dynamics and the open system dynamics is no longer unitary.

Since the dynamics is not unitary, information encoded in quantum systems usually becomes inaccessible from measurements on the system due to the interaction with the environment. On the other hand, since the dynamics of the open system depends on the initial state of the environment, open system dynamics has turned out beneficial for different purposes: Indirect *probing measurements* can be performed by making measurements on the evolved open system to gain information about the environment. High control of the initial state of the environment can be exploited to engineer the dynamics of the open system.

But how the environment should be taken into account in the physicality requirements of the open system dynamics? For the sake of example, let

us consider the simple transpose map, $|\phi_i\rangle\langle\phi_j| \xrightarrow{\mathcal{T}} (|\phi_i\rangle\langle\phi_j|)^T := |\phi_j\rangle\langle\phi_i|$ w.r.t. some fixed orthonormal basis $\{\phi_i\}_{i=1}^d$. Since transpose affects neither the diagonal elements $|\phi_i\rangle\langle\phi_i|$ nor the eigenvalues, $\mathcal{T}$ is a positive and TP map. On the other hand, any map Φ can be expanded to cover also some ancillary system E by defining a combined map $\Phi \otimes \mathcal{I}^E$ where $\mathcal{I}^E$ is the identity map of $\mathcal{H}^E$. By fixing the dimensions of S and E as $d^S = d^E = 2$, it is easy to find $\rho^{SE} \in \mathcal{S}(\mathcal{H}^{AB})$ such that $\mathcal{T} \otimes \mathcal{I}^E(\rho^{SE})$ is not a positive operator, and thus the total dynamics of SE it not physical. So we see, that positivity and TP are only necessary but not sufficient conditions for the physicality of dynamics.

Instead of concentrating on the positivity of the output states of S in the dynamics, we have to guarantee the positivity of output states of the extended systems SE where E is any ancillary system with arbitrary dimension k. So, now the physicality of the TP dynamical map Φ_t is equivalent to $\Phi_t \otimes \mathcal{I}_k \geq \mathcal{O}$, where $\mathcal{I}_k$ is the identity map of the k-dimensional Hilbert space. If $\Phi_t \otimes \mathcal{I}_k \geq \mathcal{O}$, we say that Φ_t is *k-positive*, and if Φ_t is TP and k-positive $\forall\, k$, the dynamical map describes physical state evolution and we say that it is *completely positive and trace preserving* (CPTP). For short, we call CPTP maps *quantum channels*.

If we know how the total closed system SE evolves, we can also find the reduced dynamics of S. If the initial state of SE is $\rho^{SE}(0)$, the dynamics of the reduced state $\rho^S(0)$ of S becomes

$$\rho^S(t) = \mathrm{tr}_E\big[U(t)\rho^{SE}(0)U(t)^\dagger\big] =: \sum_{i=0}^{d^E} \langle\phi_i^E|U(t)\rho^{SE}(0)U(t)^\dagger|\phi_i^E\rangle\,, \tag{2.5}$$

where $\mathrm{tr}_K[\,\cdot\,]$ is the partial trace w.r.t. system K, and $\{\phi_i^E\}_{i=0}^{d^E}$ is any orthonormal basis for E.

Suppose that the state of the closed system SE is initially uncorrelated, $\rho^{SE}(0) = \rho^S(0) \otimes \rho^E(0)$. Now we can write the reduced dynamics of the open system S in Eq. (2.5) as [37]

$$\rho^S(t) = \Phi_t(\rho^S(0)) := \mathrm{tr}_E\big[U(t)\,\rho^S(0) \otimes \rho^E(0)\,U^\dagger(t)\big]. \tag{2.6}$$

Next, let us assume that the state of the environment E is initially pure, $\rho^E = |\phi^E\rangle\langle\phi^E|$. If ρ'^E is mixed, it can always be purified with an ancillary system and by expanding its Hilbert space as $\mathcal{H}'^E \to \mathcal{H}'^E \otimes \mathcal{H}'^E := \mathcal{H}^E$.

Using this, we can write

$$\Phi_t(\rho^S(0)) = \sum_{i=1}^{d^E} \langle \phi_i^E | U(t) | \phi^E \rangle \rho^S(0) \langle \phi^E | U^\dagger(t) | \phi_i^E \rangle = \sum_{i=1}^{d_E} K_i \rho^S(0) K_i^\dagger \,, \quad (2.7)$$

where $\{\phi_i^E\}_{i=1}^{d^E}$ is an orthonormal basis for $\mathcal{H}^E$ and we have defined $K_i(t) = \langle \phi_i^E | U(t) | \phi^E \rangle$.

The representation $\Phi_t(\rho(0)) = \sum_{i=1}^{d_E} K_i \rho(0) K_i^\dagger$ is called the *Kraus decomposition* of Φ_t, and the operators K_i are called *Kraus operators*. Kraus decomposition is commonly used since it guarantees the physicality of the dynamical map: A dynamical map Φ_t is CPTP if and only if it can be represented by a Kraus decomposition [71]. This immediately tells us that any unitary map, and thus also closed system dynamics, is CPTP.

For every channel Φ_t there exists also a *complementary channel* $\tilde{\Phi}_t$ which is defined in the following way:

$$\tilde{\Phi}_t(\rho^S(0)) := \mathrm{tr}_S\big[U(t)\, \rho^S(0) \otimes \rho^E(0)\, U^\dagger(t)\big],$$

where the state of the environment $\rho^E(0)$ has again been purified as $\rho^E(0) = |\phi_E\rangle\langle\phi_E|$. Physically $\tilde{\Phi}_t(\rho^S(0))$ represents how the environment changes in the channel Φ_t when the system is initially in state $\rho^S(0)$. Similarly to the above consideration, the complementary channel can be decomposed as [72]

$$\tilde{\Phi}_t(\rho^S(0)) = \sum_{k,l=1}^{d_E} |\phi_k^E\rangle\langle\phi_l^E| \mathrm{tr}_S\Big[\rho^S(0) K_l^\dagger K_k\Big] \,. \quad (2.8)$$

In Eq. (2.4), we have written the equation of motion describing the closed system time evolution. Now, starting from the total closed system SE, we can write the *master equation*, the equation of motion for the open system S.

$$\frac{\mathrm{d}}{\mathrm{d}t}\rho^S(t) = \frac{\mathrm{d}}{\mathrm{d}t}\mathrm{tr}_E[\rho^{SE}(t)] = -\frac{i}{\hbar}\,\mathrm{tr}_E\Big[[H^{SE}(t), \rho^{SE}(t)]\Big] \quad (2.9)$$

One popular approach to studying the dynamics of open systems is

master equations of the following time-local form:

$$\frac{\mathrm{d}\rho(t)}{\mathrm{d}t} = -\frac{i}{\hbar}[H(t), \rho(t)] + \sum_i \gamma_i(t)\Big(A_i\rho(t)A_i^\dagger - \frac{1}{2}\big\{A_i^\dagger A_i, \rho(t)\big\}\Big)\,. \quad (2.10)$$

Here, $H(t)$ is the system Hamiltonian, we call A_i the Lindblad or jump operators, the time-dependent real-valued functions $\gamma_i(t)$ are called the *decay rates*, and $\{X, Y\} := XY + YX$ is the anti-commutator of operators X and Y. The solution of the master equation defines the dynamical map $\rho(t) = \Phi_t(\rho(0))$. We say that a dynamical map Φ_t is *CP-divisible* if for all $s \in [0, t]$ there exists a completely positive propagator map $V_{t,s}$ such that [37]

$$\Phi_t = V_{t,s} \circ \Phi_s\,. \quad (2.11)$$

What makes the form of master equations in Eq. (2.10) especially useful is that specifying the decay rates $\gamma_i(t)$ gives immediate information on the characteristics of Φ_t: we know that Φ_t is CP-divisible if and only if $\gamma_i(t) \geq 0 \,\forall\, t \geq 0, i$ [39]. Since all CP-divisible maps are also CP, the positivity of decay rates implies physicality of the evolution. Also, the dynamical map can be decomposed for all $s \in [0, t]$ as

$$\Phi_t = \Phi_{t-s} \circ \Phi_s \quad (2.12)$$

if and only if the decay rates are constant and positive. We call dynamical maps satisfying the condition of Eq. (2.12) *dynamical semigroups* [37, 73, 74].

When CP-divisibility is violated, it is not as straightforward to say if the solution of Eq. (2.10) is CPTP or not. Is complete positivity, or even positivity, always necessary for physical evolution? As we will see later, in the case of high control of initial correlations between the system and environment the dynamics can go beyond these restrictions.

Chapter 3

Information

Since the days of the first radio, telephone, and computer, different technologies have changed the lives of entire generations. More recently, devices and protocols exploiting quantum phenomena have attracted a lot of attention. Quantum computing, quantum communication, and quantum simulation are often seen as the possible next steps of information technology, just to name a few.

As different technological applications have different specific requirements, it is necessary to have various measures of information in order to optimize and benchmark each protocol w.r.t. the desired quantity. In this chapter, we present and discuss some commonly used measures of information. In the single-partite case, we consider information in the sense of storing and reading symbols encoded in a quantum system or the total message encoded into an ensemble of quantum states. In the bipartite case, we consider correlations between two systems. The systems can be separated either in time, as in the case of sent and received information, or space, as in entanglement between two spatially separated systems.

3.1 Single-partite systems

3.1.1 Trace distance

Commonly, information is stored, transmitted, and processed in binary form, as sequences of symbols "0" and "1". In order to store or send the information, the symbols have to be encoded in some physical information carrier. In quantum information, the different symbols can be encoded in states ρ_0 and ρ_1 of the system. The encoded information can be extracted by performing measurements on the system to figure out which symbol it

represents. So, reading the encoded data is essentially distinguishing the states ρ_0 and ρ_1. Thus, the probability of distinguishing the states can be seen as a measure of information stored in the system.

Since measurements on quantum system generally change the state irreversibly, each information carrier should be measured only once. In the case where the encoded bit is "0" or "1" with probability of 0.5, the success probability of distinguishing the states ρ_0 and ρ_1 in a single optimal measurement is $(1 + D(\rho_0, \rho_1))/2$ [75, 76] . Here, $D(\rho, \sigma)$ is the *trace distance* between states ρ and σ, defined as

$$D(\rho, \sigma) := \frac{1}{2}\mathrm{tr}\Big[|\rho - \sigma|\Big], \tag{3.1}$$

where $|X| = \sqrt{X^\dagger X}$ is the absolute value of the operator X, and $\sqrt{X}$ is the unique positive operator satisfying $\sqrt{X}\sqrt{X} = X$. In addition to its clear information theoretical interpretation, trace distance is also a proper norm in the state space.

Since trace distance quantifies the information stored in the system, increases of $D(\rho_0, \rho_1)$ indicate revivals of information, or *information back flow*. $D(\rho, \sigma)$ is contractive under positive TP maps, and thus an increase of $D(\rho_0, \rho_1)$ implies violation of P-divisibility, and as a consequence, of CP-divisibility [11]. For qubit systems, the equation of motion for the corresponding Bloch vector $\mathbf{r}(t)$ can be written as $\frac{\mathrm{d}\mathbf{r}(t)}{\mathrm{d}t} = \mathcal{D}(t)\mathbf{r}(t) + \mathbf{v}(t)$, where $\mathcal{D}(t)$ is called the damping matrix of the dynamical map, and $\mathbf{v}(t)$ the drift vector. The trace distance between the most sensitive pair of initial states increases if and only if

$$\lambda_{max}[\mathcal{D}(t)^T + \mathcal{D}(t)] > 0\,. \tag{3.2}$$

where $\lambda_{max}[X]$ is the largest eigenvalue of operator X [77].

3.1.2 Fidelity

The fidelity between a pure quantum state $|\phi\rangle\langle\phi|$ and a mixed quantum state σ, defined as

$$F(|\phi\rangle\langle\phi|, \sigma) := |\langle\phi|\sigma|\phi\rangle|\,, \tag{3.3}$$

was used as a quantum generalization of the classical fidelity of probability distributions to quantify the success rate of data transmission in pure state encoding [78]. Uhlmann called the fidelity *"transition probability"*, and it has been commonly used as a measure of how close σ is to $|\phi\rangle\langle\phi|$ [79]. In fact, the quantity in Eq. (3.3) is exactly the probability of getting the measurement outcome corresponding to $|\phi\rangle\langle\phi|$ in a measurement with POVM elements $E_1 = |\phi\rangle\langle\phi|$ and $E_2 = \mathbb{1} - |\phi\rangle\langle\phi|$ when the system is in state σ. In this sense, Eq. (3.3) acts as quantifier of how likely it is to mistake σ for $|\phi\rangle\langle\phi|$.

When generalizing fidelity for mixed states, Jozsa postulated that also the mixed state fidelity has to satisfy the following axioms:

$$\begin{aligned}
&\text{(F1)}\quad 0 \leq F(\rho,\sigma) \leq 1, \text{ and } F(\rho,\sigma) = 1 \iff \rho = \sigma\,,\\
&\text{(F2)}\quad F(\rho,\sigma) = F(\sigma,\rho)\,,\\
&\text{(F3)}\quad \text{Equation (3.3) holds for for } \rho = |\phi\rangle\langle\phi|\,,\\
&\text{(F4)}\quad F(U\rho U^\dagger, U\sigma U^\dagger) = F(\rho,\sigma) \text{ for all unitaries } U\,.
\end{aligned} \tag{3.4}$$

Jozsa showed that the mixed state generalization of fidelity, satisfying the axioms in Eq. (3.4), for mixed states ρ and σ can be chosen as [80]

$$F(\rho,\sigma) = \operatorname{tr}\left[\sqrt{\sqrt{\rho}\sigma\sqrt{\rho}}\right]^2\,, \tag{3.5}$$

In addition to satisfying the axioms in Eq. (3.4), $F(\rho,\sigma) = 0$ if and only if the supports of ρ and σ are orthogonal [11].

Even though the generalized form in Eq. (3.5) does not have similar measurement probability meaning as Eq. (3.3) it can still be given an analogous interpretation. Let P_ρ be the set of purifications of ρ and P_σ be the set of purifications of σ. Now the fidelity can be written as [80]

$$F(\rho,\sigma) = \max_{\phi\in P_\rho,\, \psi\in P_\sigma} |\,\langle\,\phi\,|\,\psi\,\rangle\,|^2\,. \tag{3.6}$$

This means that $F(\rho,\sigma)$ is the maximum probability of mistaking a purification of ρ for a purification of σ.

Despite the fact that fidelity is not a proper metric for state space, it is commonly used to quantify the closeness of quantum states [11]. In addition, it can be used to define a metric, namely the Bures distance as $D_B(\rho,\sigma) := \sqrt{2 - 2\sqrt{F(\rho,\sigma)}}$. Despite their apparent differences, fidelity

and trace distance can be linked by the following inequalities [11]

$$1 - \sqrt{F(\rho,\sigma)} \leq D(\rho,\sigma) \leq \sqrt{1 - F(\rho,\sigma)}\,. \tag{3.7}$$

3.1.3 Bloch volume

Using the generalized Bloch vector representation of N-level quantum states, one can also investigate the classical information encoded in an ensemble of quantum states from the point of view of the dynamically accessible set of states. The dynamically accessible states are all the states that can be reached by applying some CPTP map to the current set of states. We call the volume of dynamically accessible states the *Bloch volume*.

Now, we follow the reasoning of [43], according to which the Bloch volume can be linked to classical information encoded in an ensemble of quantum states. Let us assume a situation, where each symbol i is encoded at time $t = 0$ in different quantum state $\rho(\mathbf{r}_i)$ with Bloch vector $\mathbf{r}_i(0)$ and $p_0(\mathbf{r}_i(0))$ is the probability of state $\rho(\mathbf{r}_i(0))$ to appear in the ensemble. The differential entropy of the total ensemble is

$$h[p_0(\mathbf{r}(0))] := -\int_{B_N} p_0(\mathbf{r}(0)) \log_2(p_0(\mathbf{r}(0)))\mathrm{d}V_N\,, \tag{3.8}$$

where $\mathrm{d}V_N$ is the volume element of B_N, which is the set of the generalized Bloch vectors of an N-level system [1].

Let us consider the time-evolved state ensemble with the Bloch vectors at time t, given by $\mathbf{r}(t) = \mathbf{A}(t)\mathbf{r}(0) + \mathbf{q}(t)$. If a state with Bloch vector $\mathbf{r}_i(0)$ was encoded with probability $p_0(\mathbf{r}_i(0))$ at time $t = 0$, the probability of $\mathbf{r}_i(t)$ appearing in the evolved ensemble is given by $p_t(\mathbf{r}_i(t)) = p_0(\mathbf{r}_i(0))/|\det(\mathbf{A}(t))|$: since the volume of the state ensemble changes, the distribution has to be normalized as $p_t(\mathbf{r}(t)) = p_0(\mathbf{r}(0))/|\det(\mathbf{A}(t))|$, where $|\det(\mathbf{A}(t))|$ describes how the Bloch volume evolves [43]. Now, the change in differential entropy can be written as [43]

$$h[p_t(\mathbf{r}(t))] - h[p_0(\mathbf{r}(0))] = \log_2 |\det(\mathbf{A}(t))|\,. \tag{3.9}$$

[1] We note that, despite its apparent similarity with Shannon entropy, differential entropy should not be used to measure information in the ensemble, since it can become negative. Nevertheless, we discuss it for the information theoretical motivation of a geometrical characterization of quantum Markovianity, defined in [43], which will be discussed in 3.3.2.

Thus, decreasing and increasing Bloch volume implies loss and revival of differential entropy, respectively. Since the Bloch volume is contractive under positive and trace preserving maps, differential entropy can only decrease when applying CPTP maps to the ensemble [43].

In [77], it was shown that whether the Bloch volume decreases or increases, depends directly on the trace of the damping matrix $\mathcal{D}(t)$: the Bloch volume increases if and only if

$$\mathrm{tr}[\mathcal{D}(t)] > 0\,. \tag{3.10}$$

3.1.4 l_1- norm measure of coherences

Quantum coherence is an important property in many practical applications of quantum mechanics: In the BB84 quantum key distribution protocol, the coherence of elements of multiple mutually unbiased orthonormal bases is essential for success [22]. Coherence has proven useful in quantum algorithms [81, 82] and metrology [83]. Coherence even seems to be beneficial for photosynthesis [84]

To quantify the amount of coherences, multiple coherence measures have been defined [85–87]. By definition, coherence measure has to be non-increasing under incoherent CPTP maps. Here, incoherent map refers to maps that preserve diagonal states as diagonal w.r.t. some fixed basis $\mathcal{B}$ [85]. In this thesis, we restrict to a simple coherence measure, namely the l_1-norm of coherences, which is defined as [85]

$$C_{l_1}(\rho(t)) = \sum_{i \neq j} |\langle i|\rho(t)|j\rangle|\,, \tag{3.11}$$

where i, $j \in \mathcal{B}$ in the summation.

3.2 Bipartite systems

3.2.1 Mutual information

The amount of information in a message is often quantified by the probabilities $p(x)$ of symbols $x \in X$ appearing. From his intuitive axioms for a

measure of information, Shannon derived the *Shannon entropy* [88]

$$H(\{p(x)\}) := -\sum_{x\in X} p(x)\log_2 p(x)\,. \tag{3.12}$$

Shannon entropy tells how much information about the total message we obtain on average by obtaining one of its symbols, or conversely, the amount of uncertainty about the message before knowing any of the symbols [11]. According to Shannon's noiseless channel coding theorem, Shannon entropy is also the minimum amount of information as bits required in perfect transmission to encode a symbol in a message sent through a noiseless classical channel [11].

For two discrete random variables X and Y with a combined probability distribution $p(x, y)$ the *classical mutual information* is defined as [11]

$$I(X:Y) := H\big(\{p(x)\}\big) + H\big(\{p(y)\}\big) - H\big(\{p(x,y)\}\big)\,. \tag{3.13}$$

$I(X:Y)$ is the amount of information that can be deduced about the contents of X when the contents of Y is known. With the relation for combined and conditional probabilities, $p(x, y) = p(y|x)p(x)$, we can write

$$I(X:Y) = \sum_{x\in X} p_A(x) \sum_{y\in Y} p(y|x)\log_2 \frac{p(y|x)}{p_B(y)}. \tag{3.14}$$

To characterize the amount of correlations between the messages sent by Alice and received by Bob we denote the set of symbols sent by Alice with X and the set of symbols received by Bob with Y. Here, $p_A(x)$ is the probability that Alice sends the symbol x and $p_B(y)$ is the probability of Bob receiving the symbol y. $p(y|x)$ is the conditional probability of Bob receiving the symbol y when Alice sent the symbol x. When Alice and Bob agree to encode symbols $x \in X$ in quantum states ρ_x the conditional probabilities become

$$p(y|x) = \mathrm{tr}[E_y \rho_x]\,, \tag{3.15}$$

where E_y is the POVM element corresponding to the state ρ_y.

If the symbols are encoded in states with orthogonal supports and the transmission channel is noiseless, then $p(y|x) = \delta_{y,x}\ \forall x \in X,\ y \in Y$ which means error-free communication. In reality, no communication channel is

perfect so some errors are bound to happen. Different ways of fighting errors have been examined, for example error correcting codes [11, 89–92] and engineering of environments to control noise [44, 93, 94]. As we will see, controlling the environment state carefully and combining different noises can be used to return information to the system as the interaction time increases.

While in classical information theory the messages are described by probability distributions $p(x)$, in quantum information theory the probabilities are obtained from the state ρ of the system. Due to this difference, we need another measure for information in quantum systems, namely *Von Neumann entropy*

$$S(\rho) := -\mathrm{tr}[\rho \log \rho]\,, \tag{3.16}$$

the quantum generalization of Shannon entropy [11]. For a state ρ with eigenvalues λ_i, we get $S(\rho) = H(\{\lambda_i\})$. Thus, the von Neumann entropy corresponds to the Shannon entropy of measurement outcome probability distribution w.r.t. projections on the eigenbasis of the system state. A quantum equivalent of Shannon's noiseless channel coding theorem, namely the Schumacher's noiseless channel coding theorem, links the von Neumann entropy of a state $\rho = \sum_{i=1}^{n} p_i |\phi_i\rangle\langle\phi_i|$, corresponding to the quantum information source $\{p_i, \phi_i\}_{i=1}^{n}$, directly to the amount of qubits that are required to send its information content faithfully [11]. In this way, von Neumann entropy is also naturally related to information contained by the system.

For a quantum generalization of classical mutual information, let us consider the following scheme, illustrated in Fig. 3.1. The system S is initially in the state $\rho_A \in \mathcal{S}(\mathcal{H}^S)$ which is purified to ρ_{AP} by expanding its Hilbert space to $\mathcal{H}^S \otimes \mathcal{H}^P$. The change of the system in the transmission is described by $\Phi(\rho_A) = \rho_B$ and the evolved purified state is $(\Phi \otimes \mathcal{I}^P)\rho_{AP} = \rho_{BP}$. Now we can consider the following quantity called the *quantum mutual information* [72]

$$I(\rho_A, \Phi) := S(\rho_P) + S(\rho_B) - S(\rho_{BP}). \tag{3.17}$$

Equation (3.17) seems to depend essentially on the choice of the purification P, but turns out that the choice is actually irrelevant.

The dynamics of ρ_{AP} can also be described as in Eq. (2.6) by coupling it with some environment E, initially in a pure state $\rho_E \in \mathcal{S}(\mathcal{H}^E)$. Then, the

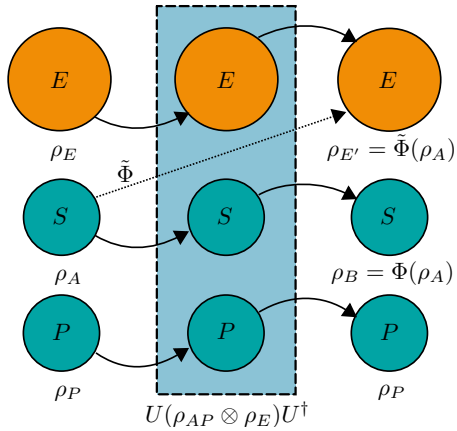

Figure 3.1: Illustration of the purifications and dynamics described by maps Φ, $\tilde{\Phi}$ and U. The state of the auxiliary system P has been chosen so that the combined state ρ_{AP} is pure and the initial state of the environment E has been chosen as pure.

total closed system APE evolves unitarily, and $\rho_{BP} = \mathrm{tr}_E\big[U(\rho_{AP}\otimes\rho_E)U^\dagger\big]$. Similarly, the environment evolves into $\rho_{E'} = \mathrm{tr}_{AP}\big[U(\rho_{AP}\otimes\rho_E)U^\dagger\big]$.

The von Neumann entropy is invariant in unitary transformations, and the dynamics of the total system APE, is unitary. The subsystems of any bipartite system in pure state have equal von Neumann entropy. Since the initial states of AP and E are pure, the total state $\rho_{AP}\otimes\rho_E$ is also pure. In addition, the entropy of the reduced state of the purification P is invariant in the dynamics. By denoting $\rho := \rho_A$, and using the above observations, we can rewrite Eq. (3.17) as

$$I(\rho, \Phi) = S(\rho) + S(\Phi(\rho)) - S(\tilde{\Phi}(\rho))\,. \tag{3.18}$$

The above expression for the quantum mutual information now depends only on the channel and the initial state of the system. Thus, we conclude that the choice of the purifying state ρ^P is irrelevant. Quantum mutual information satisfies the *data processing inequality* [72]:

$$I(\rho, \Phi) \geq I(\rho, \Phi' \circ \Phi)\,, \tag{3.19}$$

for any channels Φ and Φ'. In other words, concatenating CPTP maps can never increase quantum mutual information.

3.2.2 Coherent information

Quantum coherent information tells how much quantum information can be transferred in a noisy quantum channel [95]. For the channel Φ, visualized in Fig. 3.1, the *quantum coherent information* is defined as

$$I_c(\rho, \Phi) := S(\rho_B) - S(\rho_{PB}). \tag{3.20}$$

In the same way as for mutual information, the coherent information can be written in the form:

$$I_c(\rho, \Phi) = S\big(\Phi(\rho)\big) - S\big(\tilde{\Phi}(\rho)\big)\,. \tag{3.21}$$

For any channels Φ and Φ', coherent information satisfies the *quantum data processing inequality* [95]:

$$I_c(\rho, \Phi) \geq I_c(\rho, \Phi' \circ \Phi)\,, \tag{3.22}$$

which means that the coherent information never increases under CPTP maps.

3.2.3 Channel capacities

Entanglement-assisted classical capacity

For a given channel Φ the *entanglement-assisted classical capacity* $C_{ea}(\Phi)$ gives the upper-limit to the rate at which classical information can be sent through the channel Φ with help of entanglement. It is the average of the suprema of quantum mutual information in infinite consecutive uses of the channel. Here, it is assumed that the channel is memoryless, i.e., that consecutive uses of the channel form a separable map $\Phi^{\otimes n} : \bigotimes_{k=1}^{n} \mathcal{H}^k \to \bigotimes_{k=1}^{n} \mathcal{H}^k$ where each $\Phi^k : \mathcal{H}^k \to \mathcal{H}^k$ acts identically and independently of the others. Formally, we write

$$C_{ea}(\Phi) = \lim_{n\to\infty} \left[\sup_{\rho^{1,2,\ldots,n}} I(\rho^{1,2,\ldots,n}, \Phi^{\otimes n})/n \right]. \tag{3.23}$$

Here we denote the density matrices in Hilbert space $\mathcal{H}^k$ as ρ^k and density matrices in the combined Hilbert space $\bigotimes_{k=1}^n \mathcal{H}^k$ as $\rho^{1,2,\ldots,n}$. In [96] it was shown that for a channel $\Phi^{1\otimes 2} = \Phi^1 \otimes \Phi^2$ the maximization over the initial states can be written as

$$\sup_{\rho^{1,2}} I(\rho^{1,2}, \Phi^{1\otimes 2}) = \sup_{\rho^1} I(\rho^1, \Phi^1) + \sup_{\rho^2} I(\rho^2, \Phi^2). \tag{3.24}$$

Thus, we get $\sup_{\rho^{1,2,\ldots,n}} I(\rho^{1,2,\ldots n}, \Phi^{\otimes n}) = \sum_{k=1}^n \sup_{\rho^k} I(\rho^k, \Phi^k)$. Since the channel in consecutive uses is identical, $\sup_{\rho^j} I(\rho^j, \Phi^j) = \sup_{\rho^k} I(\rho^k, \Phi^k)$ for all j and k. With these observations, the entanglement-assisted channel capacity can be written as

$$C_{ea}(\Phi) = \sup_{\rho} I(\rho, \Phi). \tag{3.25}$$

Thus, we conclude that it is sufficient to perform the optimization only in terms of one use of the channel Φ.

Quantum capacity

The *quantum capacity* $Q(\Phi)$ of channel Φ is the maximum amount of quantum information that can be transmitted in a single use of Φ with asymptotically vanishing error. Similarly to the entanglement assisted capacity, the quantum capacity is given by

$$Q(\Phi) = \lim_{n\to\infty} \left[\sup_{\rho^{1,2,\ldots n}} I_c(\rho^{1,2,\ldots n}, \Phi^{\otimes n})/n \right], \tag{3.26}$$

where $I_c(\rho^{1,2,\ldots n}, \Phi^{\otimes n})$ is the coherent information calculated for n consecutive uses of the channel when sending state $\rho^{1,2,\ldots n}$. Since the coherent information is generally not additive, the optimization in Eq. (3.26) becomes complicated. For a more useful form, let us restrict to a subclass of CPTP maps.

Let the complementary channel of Φ be $\tilde{\Phi}$. If there exists a CPTP map Υ, such that $\tilde{\Phi} = \Upsilon \circ \Phi$, we say that Φ is *degradable*. For degradable channels Eq. (3.26) can be simplified as [97]

$$Q(\Phi) = \sup_{\rho} I_c(\rho, \Phi), \tag{3.27}$$

which is more practical than Eq. (3.26), since optimizing over the set of initial states for a single use of the channel is sufficient.

3.2.4 Entanglement

A genuinely quantum correlation, namely entanglement between the subsystems A and B of a bipartite system AB is a characteristic feature of quantum mechanics. Entanglement enables counter intuitive quantum phenomena, such as violation of local realism, and it is an essential ingredient in many quantum information protocols, such as quantum teleportation, superdense coding, and entanglement based quantum key distribution [13, 18, 23, 24].

The entanglement of a bipartite pure state $|\phi^{AB}\rangle$ is quantified by *entropy of entanglement* [15]

$$E(\phi^{AB}) := S(\mathrm{tr}_A[\phi^{AB}]) = S(\mathrm{tr}_B[\phi^{AB}]) \tag{3.28}$$

For bipartite mixed states, entanglement can be quantified by the generalization of entropy of entanglement, namely *entanglement of formation* [16]

$$E(\rho^{AB}) := \min_{\{p_i,\phi_i^{AB}\}_i} \sum_i p_i E(\phi_i^{AB})\,, \tag{3.29}$$

where $\{p_i, \phi_i^{AB}\}_i$ satisfies $\rho^{AB} = \sum_i p_i \phi_i^{AB}$, $\sum_i p_i = 1$, $p_i \in [0,1]$, and ϕ_i^{AB} are pure states, for all i. In other words, entanglement of formation is the minimum amount of weighted average entanglement required in its pure state decomposition.

Wootters showed that for a two-qubit state ρ^{AB}, entanglement of formation can be calculated as

$$E(\rho^{AB}) = h_2\left[\left(1+\sqrt{1-C(\rho^{AB})^2}\right)/2\right], \tag{3.30}$$

$$h_2[x] := -x\log_2(x) - (1-x)\log_2(1-x)\,, \quad \text{and} \tag{3.31}$$

$$C(\rho^{AB}) := \max\{0, \lambda_1 - \lambda_2 - \lambda_3 - \lambda_4\}\,. \tag{3.32}$$

Here $h_2[x]$ is called the *binary Shannon entropy* and $C(\rho^{AB})$ is the *concur-*

rence of ρ^{AB}. The λ_k's are the eigenvalues of the matrix

$$\sqrt{\sqrt{\rho^{AB}}(\sigma_2 \otimes \sigma_2)(\rho^{AB})^*(\sigma_2 \otimes \sigma_2)\sqrt{\rho^{AB}}} \tag{3.33}$$

ordered in the decreasing order, and X^* is an operator whose elements are given by $\langle ij|X^*|kl\rangle = \langle ij|X|kl\rangle^*$, where $i, j, k, l \in \{0, 1\}$ [16]. In addition to entanglement of formation, also concurrence is commonly used as entanglement measure for two-qubit systems.

3.2.5 Non-locality

In addition to its many practical applications, entanglement also leads to fundamental differences between the classical and quantum description of Nature. In their famous paper, Einstein, Podolsky, and Rosen presented their criticism against the completeness of quantum theory [17]. They postulated that *if, without in any way disturbing a system, we can predict with certainty the value of a physical quantity, then there exists an element of physical reality corresponding to this physical quantity.* In complete theory, *every element of the physical reality must have a counterpart in the physical theory.* By using entangled states of combined system AB, they showed that there exist two measurements $\hat{a}$ and $\hat{a}'$ on the subsystem A, measuring which gives immediately certain prediction of the outcomes of two non-commuting observables $\hat{b}$ and $\hat{b}'$ of subsystem B, respectively. Thus, to be a complete theory, the definite outcome of $\hat{b}$ and $\hat{b}'$ should have simultaneous counterparts in quantum mechanics, or measurements on A should be able to disturb system B no matter how far apart they are.

By assuming that hidden-variable theory, containing the elements of the physical reality, is local Clauser, Horne, Shimony and Holt derived the so-called CHSH inequality, which can be used to test the compatibility of local hidden-variable theories with experimental observations [18]. In quantum mechanics, when the system AB is in state ρ the CHSH inequality implies

$$\mathfrak{B}_{CHSH} \leq 2\,, \quad \text{where} \tag{3.34}$$

$$\mathfrak{B}_{CHSH} = \max_{\hat{a},\,\hat{a}',\,\hat{b},\,\hat{b}'} \left|\mathrm{tr}[\rho(\hat{a} \otimes (\hat{b} + \hat{b}') + \hat{a}' \otimes (\hat{b} - \hat{b}'))]\right| \tag{3.35}$$

is the *Bell function* and the subsystems A and B are spacelike separated. Here $\hat{a}$ and $\hat{a}'$ are some observables of qubit A, and $\hat{b}$ and $\hat{b}'$ are some ob-

servables of qubit B which all have exactly -1 and $+1$ as possible outcomes. Whenever $\mathfrak{B}_{CHSH} > 2$, the locality assumption of the hidden variable theories is violated, and we say that *the state is non-local*. After its inception, CHSH inequality has been repeatedly violated in experiments, suggesting that the local hidden variable theories cannot accurately describe the observable reality [19–21].

For 2-qubit systems the Bell function simplifies to

$$\mathfrak{B}_{CHSH} = 2\sqrt{u + \tilde{u}}\,. \tag{3.36}$$

Here u and $\tilde{u}$ are the two largest eigenvalues of $M_\rho^{\mathrm{T}} M_\rho$, and $M_{i,j} = \mathrm{tr}[\rho\sigma_i \otimes \sigma_j]$ for $i, j \in \{1, 2, 3\}$ [98].

3.3 Markovianity

In this section, we'll concentrate on Markovianity and non-Markovianity, properties of dynamical maps characterizing the loss and revival of information in the information carrier.

3.3.1 Classical Markovianity

Let X be a random variable which has value $X(t_k) = x_k \in \mathcal{X}$ at time $t_k \in I$ where $\mathcal{X}$ is some fixed set and I is some time interval. A classical stochastic process $\{X(t), t \in I\}$ is *Markovian* if for all $\{t_n \geq t_{n-1} \geq ... \geq t_0\} \subset I$

$$P(x_n, t_n | x_{n-1}, t_{n-1}; ...; x_0, t_0) = P(x_n, t_n | x_{n-1}, t_{n-1}) \ , \tag{3.37}$$

Here $P(x_n, t_n | x_{n-1}, t_{n-1}; ...; x_0, t_0)$ is the probability that $X(t_n) = x_n$ in the condition that $X(t_{n-1}) = x_{n-1}, X(t_{n-2}) = x_{n-2}, ..., X(t_0) = x_0$ [46]. In other words, a Markovian stochastic process does not have memory of the previous values of $X(t)$.

Let us consider the *transition matrix* T which connects the one-time probabilities of $X(t_2) = x_2$ and $X(t_1) = x_1$, where $t_2 \geq t_1$ and $t_1, t_2 \in I$ in the following way:

$$P(x_2, t_2) = \sum_{x_1 \in \mathcal{X}} T(x_2, t_2 | x_1, t_1) P(x_1, t_1). \tag{3.38}$$

Since $P(x, t_2)$ has to be a probability distribution for any probability dis-

tribution $P(x, t_1)$, T has to be a *stochastic matrix*, meaning that it must satisfy

$$\begin{aligned} T(x_2, t_2|x_1, t_1) &\geq 0 \ \ \forall x_1, x_2 \in \mathcal{X}, \ \text{ and} \\ \sum_{x_2 \in \mathcal{X}} T(x_2, t_2|x_1, t_1) &= 1 \ \ \forall x_1 \in \mathcal{X}. \end{aligned} \tag{3.39}$$

We call a stochastic process $\{X(t), t \in I\}$ *divisible* if for all $t_0, t_1, t_2, t_3 \in I$ such that $t_0 \leq t_1 \leq t_2 \leq t_3$ its transition matrix T satisfies

$$T(x_3, t_3|x_1, t_1) = \sum_{x_2 \in \mathcal{X}} T(x_3, t_3|x_2, t_2) T(x_2, t_2|x_1, t_1)\,. \tag{3.40}$$

Any Markovian stochastic process satisfies Eq. (3.40), and thus all Markovian processes are divisible. On the other hand, there exist divisible non-Markovian stochastic processes. So, in general for classical stochastic processes, Markovianity and divisibility are not equivalent but in the case of one-time probabilities $P(x, t)$ divisibility and Markovianity become equivalent [46].

3.3.2 Quantum Markovianity

Finding a quantum equivalent for the classical definition of Markovianity turns out to be problematic. This is due to the fact that measurements on a quantum object at time t_1 disturb the state and thus influence the probabilities of different measurement outcomes at times $t_2 \geq t_1$. This means that using two different measurement schemes could lead to different forms of $P(x_n, t_n|x_{n-1}, t_{n-1}; ...; x_0, t_0)$. Thus, any such definition of quantum Markovianity would depend on the choice of the measurement sequence while Markovianity should be purely a property of the dynamics. In this subsection, we will first discuss one of the commonly used definitions for quantum Markovianity, following the terminology and motivation of [46]. Then, we recall some definitions based on the lack of memory in the dynamics.

By performing state tomography, the density matrix of the system can be constructed at all $t \in I$. Thus the one-time probabilities $P(x, t)$ can be obtained even for a quantum process. This can be done without having problems caused by the disturbing nature of measurements. Let $\rho(t_0)$ be the density matrix of some state at time t_0. We can write it in its eigenbasis

as

$$\rho(t_0) = \sum_{x_0 \in \mathcal{X}} p(x_0, t_0) |\psi_{x_0}\rangle\langle\psi_{x_0}|, \tag{3.41}$$

for some countable index set $\mathcal{X}$. Here the eigenvalues $p(x_0, t_0)$ form a classical probability distribution and each $p(x_0, t_0)$ is a probability of ψ_{x_0} to appear in the ensemble $\rho(t_0)$ at the time t_0, $P(\psi_{x_0}, t_0) = p(x_0, t_0)$.

Let us suppose that the system experiences some eigenbasis preserving dynamics $\rho(t_0) \xrightarrow{\Phi_{t_1,t_0}} \rho(t_1)$ where Φ_{t_1,t_0} is a CPTP map and

$$\Phi_{t_1,t_0}\big(\rho(t_0)\big) = \rho(t_1) = \sum_{x_1 \in \mathcal{X}} p(x_1, t_1) |\psi_{x_1}\rangle\langle\psi_{x_1}|, \tag{3.42}$$

meaning that the eigenstates $|\psi_x\rangle$ don't change in time but the corresponding eigenvalues $p(x, t)$ can evolve. Here $p(x_1, t_1)$ is some other classical probability distribution of the random variable x_1 at time t_1. On the other hand the evolution in Eq. (3.42) is also a classical stochastic process of the random variable $x \in \mathcal{X}$. This means we can write the probabilities $p(x, t)$ by using the transition matrix T:

$$p(x_1, t_1) = \sum_{x_0 \in \mathcal{X}} T(x_1, t_1 | x_0, t_0) p(x_0, t_0). \tag{3.43}$$

If the classical stochastic process of one-time probabilities is also divisible, and thus Markovian, we can combine equations (3.42), and (3.43) with the divisibility condition Eq. (3.40) which gives

$$\begin{aligned}
\Phi_{t_2,t_0}(\rho(t_0)) &= \sum_{x_2 \in \mathcal{X}} p(x_2, t_2) |\psi_{x_2}\rangle\langle\psi_{x_2}| \\
&= \sum_{x_2, x_0 \in \mathcal{X}} T(x_2, t_2 | x_0, t_0) p(x_0, t_0) |\psi_{x_2}\rangle\langle\psi_{x_2}| \\
&= \sum_{x_2, x_1, x_0 \in \mathcal{X}} T(x_2, t_2 | x_1, t_1) T(x_1, t_1 | x_0, t_0) p(x_0, t_0) |\psi_{x_2}\rangle\langle\psi_{x_2}| \\
&= \Phi_{t_2,t_1}\left(\sum_{x_1, x_0 \in \mathcal{X}} T(x_1, t_1 | x_0, t_0) p(x_0, t_0) |\psi_{x_1}\rangle\langle\psi_{x_1}| \right) \\
&= \Phi_{t_2,t_1} \circ \Phi_{t_1,t_0}\big(\rho(t_0)\big)\,.
\end{aligned} \tag{3.44}$$

To guarantee physicality of the dynamics, we require that Φ_{t_1,t_0} and Φ_{t_2,t_1} are CP maps. Equation (3.44) shows that if the classical process describing the evolution of the one-time probabilities in the eigenbasis is Markovian, the CPTP map Φ_{t_2,t_0} can be decomposed at arbitrary times $t_1 \in [t_0, t_2]$ into $\Phi_{t_2,t_0} = \Phi_{t_2,t_1} \circ \Phi_{t_1,t_0}$ [46]. Such processes were defined in Section 2.2.2 as CP divisible.

More generally, CP divisibility has been suggested as a definition for Markovianity of quantum dynamical map [46]. If the dynamical map is not Markovian, we say it is non-Markovian. If the master equation is written in form of Eq. (2.10), the dynamics is Markovian if and only if $\gamma_k(t) \geq 0 \ \forall \ t \geq 0 \ \forall \ k$ [73, 74]. For example, unitary dynamics is always Markovian since $\gamma_k(t) = 0 \ \forall \ t \geq 0 \ \forall \ k$.

Since the above construction depends on restricting to one-time probabilities and assumes that the dynamical map preserves the eigenbasis, it is not a perfect generalization of classical Markovianity. Multiple different definitions of Markovianity have been developed based on the information theoretical interpretation of classical Markovianity, namely the lack of memory on previous times [47–49, 99]. In such definitions, some information measure which is contractive under CPTP maps is fixed and dynamics is characterized as Markovian if the quantity decreases at all times of the dynamics. Thus, non-Markovianity corresponding to such definition can also be seen as indicator of violation of CP divisibility.

Due to their contractivity under CPTP maps, trace distance, Bloch volume, coherence measures, entanglement-assisted classical capacity and quantum capacity have been used to define Markovianity as their monotonic behavior [42–45]. If any of these quantities increases at some time, the information flow w.r.t. the said measure manifests memory effect and dynamics is non-Markovian in terms of that information measure.

Also non-Markovianity measures quantifying explicitly the information back-flow in dynamical processes have been defined as the amount of temporal increases of these information measures. The most commonly used measure of non-Markovianity is the so-called *BLP measure*, which is defined as total increases of trace distance [42]:

$$\mathcal{N}_{BLP}(\Phi_t) := \max_{\rho_1(0),\rho_2(0)} \int_{\dot{D}(\rho_1(t),\rho_2(t))>0} \dot{D}(\rho_1(t), \rho_2(t))\mathrm{d}t\,, \tag{3.45}$$

where the optimization is performed over all initial pairs of states. Also the

entanglement assisted and quantum channel capacities have been used to quantify non-Markovianity as temporal increases of transmission efficiency in terms of the channel capacities with the so-called *BCM measures* [44]:

$$\mathcal{N}^{ea}_{BCM}(\Phi_t) := \int_{\dot{C}_{ea}(\Phi_t)>0} \dot{C}_{ea}(\Phi_t)\mathrm{d}t\,, \tag{3.46}$$

$$\mathcal{N}^{Q}_{BCM}(\Phi_t) := \int_{\dot{Q}(\Phi_t)>0} \dot{Q}(\Phi_t)\mathrm{d}t\,. \tag{3.47}$$

Chapter 4

Phase-Covariant Master Equations

4.1 Phase-covariant qubit dynamics

From now on, we concentrate on the most general class of dynamical maps describing *phase covariant noise*. Here phase covariant refers to dynamical maps Φ_t that commute with rotations $\mathcal{U}(t)$ w.r.t. the z-axis of Bloch sphere, or more formally $\Phi_t \circ \mathcal{U}(t) = \mathcal{U}(t) \circ \Phi_t$. As shown in [100], all physical master equations for a single qubit phase covariant dynamics are of the form:

$$\frac{\mathrm{d}\rho(t)}{\mathrm{d}t} = -i\frac{\omega(t)}{2}[\sigma_3, \rho(t)] + \sum_{i=1}^{3} \frac{\gamma_i(t)}{2}\left(A_i\rho(t)A_i^\dagger - \frac{1}{2}\left\{A_i^\dagger A_i, \rho(t)\right\}\right) , \quad (4.1)$$

where

$$A_1 = \sigma_+ := (\sigma_1 + i\sigma_2)/2\,, \quad A_2 = \sigma_- := (\sigma_1 - i\sigma_2)/2\,, \quad A_3 = \sigma_3\,. \quad (4.2)$$

Here $\gamma_1(t)$, $\gamma_2(t)$, and $\gamma_3(t)$ correspond to heating, dissipation and pure dephasing of the qubit, respectively.

The phase covariant family of master equations describes a large variety of different types of dynamical maps. The dynamics is unital, meaning $\Phi_t(\frac{1}{2}\mathbb{1}) = \frac{1}{2}\mathbb{1}$, if and only if $\gamma_1(t) = \gamma_2(t)$, so the solutions include both unital and non-unital maps. For example, choosing $\gamma_1(t) = \gamma_2(t) = 0$ leads to pure dephasing dynamics, $\gamma_1(t) = \gamma_3(t) = 0$ to amplitude damping, and $\gamma_1(t) = \gamma_2(t) = 2\gamma_3(t)$ to depolarizing dynamics. For arbitrary initial qubit

state $\rho(0)$, the solution of equation (4.1) is given by

$$\Phi_t(\rho(0)) = \rho(t) = \begin{pmatrix} 1 - P_1(t) & \alpha(t) \\ \alpha^*(t) & P_1(t) \end{pmatrix}, \tag{4.3}$$

where

$$P_1(t) = \mathrm{e}^{-\Gamma(t)}[G(t) + P_1(0)], \quad \alpha(t) = \alpha(0)\mathrm{e}^{i\Omega(t) - \Gamma(t)/2 - \tilde{\Gamma}(t)}, \tag{4.4}$$

and

$$\begin{aligned} \Gamma(t) &= \frac{1}{2}\int_0^t \gamma_1(\tau) + \gamma_2(\tau)\mathrm{d}\tau, \quad \tilde{\Gamma}(t) = \int_0^t \gamma_3(\tau)\mathrm{d}\tau, \\ G(t) &= \frac{1}{2}\int_0^t \mathrm{e}^{\Gamma(\tau)}\gamma_2(\tau)\mathrm{d}\tau, \qquad \Omega(t) = \int_0^t 2\omega(\tau)\mathrm{d}\tau. \end{aligned} \tag{4.5}$$

Thus, the role of $\gamma_1(t)$, $\gamma_2(t)$, and $\gamma_3(t)$ in dephasing is additive and identical.

Let us express the dynamics in terms of components of the Bloch vector as $\rho(t) = \frac{1}{2}\left(\mathbb{1} + \sum_{i=1}^3 r_i(t)\sigma_i\right)$. The evolution of the Bloch vector is given by

$$\mathbf{r}(t) = \mathbf{A}(t)\mathbf{r}(0) + \mathbf{q}(t), \tag{4.6}$$

where $\mathbf{q}(t) = (0, 0, q_3(t))^T$,

$$q_3(t) = -e^{-\Gamma(t)}[1 + 2G(t)] + 1, \tag{4.7}$$

and the eigenvalues of the matrix $\mathbf{A}(t)$ are

$$\lambda_1(t) = \lambda_2(t)^* = e^{-\Gamma(t)/2 - \tilde{\Gamma}(t) + i\Omega(t)}, \quad \lambda_3(t) = e^{-\Gamma(t)}. \tag{4.8}$$

The dynamical map is CP if and only if all the following conditions are

satisfied [101, 102] .

$$\begin{aligned} |p_1(t)|, |p_2(t)| &\leq \frac{1}{2}, \\ y(t)^2 &\leq \left(\frac{1}{2} - p_1(t)\right)\left(\frac{1}{2} + p_2(t)\right), \\ w(t)^2 &\leq \left(\frac{1}{2} - p_2(t)\right)\left(\frac{1}{2} + p_1(t)\right), \end{aligned} \tag{4.9}$$

where

$$\begin{aligned} p_1(t) &= \frac{1}{2}[t_3(t) + \lambda_3(t)], \quad p_2(t) = \frac{1}{2}[t_3(t) - \lambda_3(t)], \\ w(t) &= \frac{1}{2}[\lambda_1(t) + \lambda_2(t)], \quad y(t) = \frac{1}{2}[\lambda_1(t) - \lambda_2(t)]. \end{aligned} \tag{4.10}$$

By applying these conditions, we see that the phase covariant dynamics is CP if and only if

$$0 \leq e^{-\Gamma(t)}\left(G(t) + 1\right) \leq 1\,, \tag{4.11}$$

$$0 \leq e^{-\Gamma(t)} G(t) \leq 1\,, \tag{4.12}$$

$$-e^{-\Gamma(t)-2\tilde{\Gamma}(t)}\sin^2\Omega(t) \leq e^{-\Gamma(t)} G(t)\Big[1 - e^{-\Gamma(t)}(G(t)+1)\Big]\,, \quad \text{and} \tag{4.13}$$

$$e^{-\Gamma(t)-2\tilde{\Gamma}(t)}\cos^2\Omega(t) \leq e^{-\Gamma(t)}\Big[1 - e^{-\Gamma(t)}G(t)\Big]\left[G(t)+1\right]. \tag{4.14}$$

We notice that the validity of Eq. (4.11) and (4.12) implies Eq. (4.13), as the l.h.s. of the inequality is always non-positive and the r.h.s. never negative. Thus, it suffices to check the conditions of Eq. (4.11), (4.12), and (4.14).

4.2 Memory effects

4.2.1 Trace distance

For the phase covariant master equation (4.1), the damping matrix $\mathcal{D}(t)$, describing dynamics of the Bloch vector as $\dot{\mathbf{r}}(t) = \mathcal{D}(t)\mathbf{r}(t) + \mathbf{v}(t)$, becomes

$$\mathcal{D}(t) = \begin{pmatrix} -\frac{\gamma_1(t)}{4} - \frac{\gamma_2(t)}{4} - \gamma_3(t) & -\omega(t) & 0 \\ \omega(t) & -\frac{\gamma_1(t)}{4} - \frac{\gamma_2(t)}{4} - \gamma_3(t) & 0 \\ 0 & 0 & -\frac{\gamma_1(t)}{2} - \frac{\gamma_2(t)}{2} \end{pmatrix}. \tag{4.15}$$

Thus, the eigenvalues of $\mathcal{D}(t)^T + \mathcal{D}(t)$ are

$$\lambda_1 = \lambda_2 = -[\gamma_1(t) + \gamma_2(t) + 4\gamma_3(t)]/2\,, \quad \lambda_3 = -[\gamma_1(t) + \gamma_2(t)]\,. \tag{4.16}$$

Now the condition in Eq. (3.2) is equivalent to

$$\gamma_1(t) + \gamma_2(t) + 4\gamma_3(t) < 0\,, \quad \text{or} \tag{4.17}$$

$$\gamma_1(t) + \gamma_2(t) < 0\,. \tag{4.18}$$

If either of these holds, then for at least one pair of initial states the trace distance increases. Since increases in trace distance are equivalent to information back flow, this means that the dynamics is non-Markovian w.r.t. the trace distance based BLP measure of non-Markovianity.

We note, that the first condition involves all the decay rates. This means that the dynamics is not detected as non-Markovian w.r.t. the first condition in cases where one or two of the decay rates are negative and others have large enough positive values to compensate the negativity. On the other hand, the second condition depends on the relation between the heating and dissipation rate but not on the pure dephasing rate. This means that there is no information back flow w.r.t. the second condition if one of the decay rates is positive and large enough to compensate the possible negativity of the other.

4.2.2 Bloch volume

In phase covariant dynamics, the Bloch volume increases if and only if

$$\mathrm{tr}[\mathcal{D}(t)] > 0 \quad \Leftrightarrow \quad \gamma_1(t) + \gamma_2(t) + 2\gamma_3(t) < 0\,. \tag{4.19}$$

This condition is always weaker than the two given by trace distance: If $\gamma_1(t) + \gamma_2(t) < 0$ trace distance increases, as seen from Eq. (4.18), but the Bloch volume might not increase depending on $\gamma_3(t)$. On the other hand, if the violation of CP divisibility is caused by the negativity of $\gamma_3(t)$, then condition Eq. (4.17) of trace distance is satisfied before condition Eq. (4.19) for Bloch volume, since the contribution of $\gamma_3(t)$ is greater in the trace distance condition.

To conclude the above, trace distance always increases for some pair of initial states if the Bloch volume increases. The result is as expected, since Bloch volume can increase only if the distance between some states increases. Contrary to this, increasing trace distance between some pair of states does not imply increases in Bloch volume, as other sets of states may simultaneously contract aggressively, resulting to decreasing Bloch volume. This means that the BLP measure is more sensitive in detecting non-Markovianity than the geometric non-Markovianity measure which is based on increases of Bloch volume.

4.2.3 l_1 norm measure of coherences

To study the coherence measure, we use the basis $\{|0\rangle, |1\rangle\}$. The coherence measures can be used as all phase covariant dynamical maps are incoherent in the chosen basis. In this case, we have

$$\frac{\mathrm{d}}{\mathrm{d}t} C_{l_1}(\rho(t)) = -\left(\frac{\gamma_1(t) + \gamma_2(t)}{2} + 2\gamma_3(t)\right) |\alpha(0)| \mathrm{e}^{-\Gamma(t)/2 - \tilde{\Gamma}(t)}\,. \tag{4.20}$$

The dynamics is non-Markovian w.r.t. the l_1-norm measure of coherences, if and only if the coherence measure increases in time. This is equivalent to

$$\frac{\mathrm{d}}{\mathrm{d}t} C_{l_1}(\rho(t)) > 0 \quad \Leftrightarrow \quad \gamma_1(t) + \gamma_2(t) + 4\gamma_3(t) < 0\,. \tag{4.21}$$

This coincides with the first information back flow condition (4.17) of trace distance, but does not consider the relation between $\gamma_1(t)$ and $\gamma_2(t)$ inde-

Table 4.1: Conditions for memory effects occurring w.r.t. different quantities.

Quantity	Memory effect occurs if and only if
Trace distance	$\min\{\gamma_1(t)+\gamma_2(t),\, \gamma_1(t)+\gamma_2(t)+4\gamma_3(t)\} < 0$
Bloch volume	$\gamma_1(t)+\gamma_2(t)+2\gamma_3(t) < 0$
Coherence measure	$\gamma_1(t)+\gamma_2(t)+4\gamma_3(t) < 0$

pendently of $\gamma_3(t)$. However, this is different than the condition of Bloch volume increasing, since the weight factor of $\gamma_3(t)$ is smaller in Eq. (4.19). The l_1-norm measure is more sensitive to the negativity of $\gamma_3(t)$, but the Bloch volume is more prone to increase when $\gamma_1(t)+\gamma_2(t) < 0$.

In Table 4.1 we collect the conditions for each type of memory effect to occur and Fig. 4.1 illustrates the relations of the different types of information back flows in the $(\gamma_1(t)+\gamma_2(t),\, \gamma_3(t))$ space. In the phase-covariant dynamics, similar results can be obtained for various other measures for non-Markovianity, namely entropy production, purity, eigenvalues of the dynamical map, and singular values of the dynamical map. For each of these, the crossovers of memory effects in the $(\gamma_1(t)+\gamma_2(t),\, \gamma_3(t))$ space are given as combinations of the conditions in Tab. 4.1.

We note that in the lower right region of Fig. 4.1, there exists an area $\gamma_3(t) < 0$, $\gamma_1(t)+\gamma_2(t)+4\gamma_3(t) \geq 0$, where the dynamics is not CP divisible since one of the decay rates is negative, but none of the memory effects occur. Equivalently, none of the corresponding non-Markovianity measures identifies the dynamics as non-Markovian for any such values. For any bounded $\gamma_3(t)$, the rates $\gamma_1(t)$ and $\gamma_2(t)$ can be chosen so that $\gamma_1(t)+\gamma_2(t)+4\gamma_3(t) \geq 0, \forall t$. This means, that violation of CP-divisibility caused by $\gamma_3(t)$ of any magnitude will not lead to any of the above mentioned memory effets if $\gamma_1(t)+\gamma_2(t)$ is large enough. An example case of such dynamics is the *Eternal non-Markovianity dynamics*, which rises from our master equation (4.1), with the choices $\gamma_1(t) = \gamma_2(t) = 2$ and $\gamma_3(t) = -\tanh(t)$ [77]. Similarly, the negativity of $\gamma_1(t)$ (or $\gamma_2(t)$) can be compensated by choosing large enough $\gamma_3(t)$ and $\gamma_2(t)$ (or $\gamma_1(t)$). Hence the potential memory effect enabled by negativity of one decay rate, can

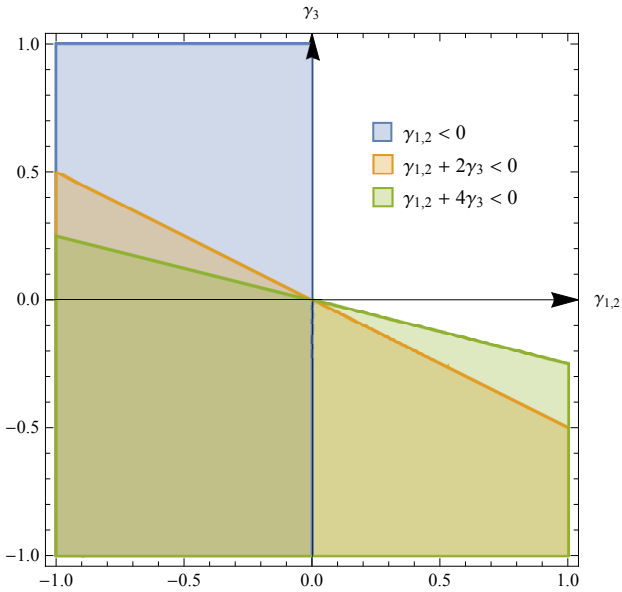

Figure 4.1: Comparison of the emergence of memory effects in the $(\gamma_1(t) + \gamma_2(t), \gamma_3(t))$ space. We have denoted $\gamma_{1,2} := \gamma_1(t) + \gamma_2(t)$.

be suppressed by increasing the others.

Chapter 5

Controlling and Measuring with Dynamics

Equation (2.6) shows how the dynamics of an open system S depends on the initial state of the environment E. It is clear that preparing E in different states ξ_1 and ξ_2 and coupling it to S with the same unitary U can induce different channels Φ_1 and Φ_2 to S. We begin this chapter by constructing a mathematical tool based on the comparison between the initial environment states and the dynamical maps they induce. Then we show how the tool can be used to achieve different tasks.

The connection between the environment state ξ and channel Φ can be exploited in *quantum probing*: Since the dynamical map Φ_t of S depends on the choice of ξ, measurements on the evolved state $\Phi_t(\rho)$ can be used to extract information on ξ. Commonly, probing protocols are based on perfect knowledge of U, but can some information be obtained even in complete ignorance of the coupling?

Intentionally controlling Φ_t with suitable choices of inducing state ξ is known as *reservoir engineering*. If the analytical solution for Φ_t is known for any ξ, also all of its characteristic properties, such as information back flow and coherence trapping can be directly deduced. What characteristics the dynamics induced by ξ_2 can be guaranteed to have if the solution for only some other inducing state ξ_1 is known? What are the ultimate limitations of reservoir engineering? If the initial correlations between S and E can be controlled with high precision, can even the positivity of the dynamics be violated at will?

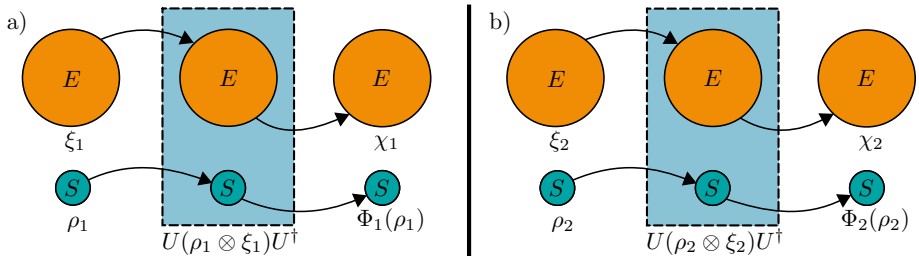

Figure 5.1: Open system S interacting with its environment E. In a) and b), the initial states of S and E are different. Even though in both cases the unitary coupling U between S and E is the same, the induced channels Φ_1 and Φ_2 may be different, since $\xi_1 \neq \xi_2$.

5.1 Limitations of reservoir engineering and their implications to probing measurements

We begin by defining the *α-fidelity of states* as

$$F_\alpha(\rho_1, \rho_2) := \mathrm{tr}\left[\left(\rho_2^{\frac{1-\alpha}{2\alpha}}\,\rho_1\,\rho_2^{\frac{1-\alpha}{2\alpha}}\right)^\alpha\right] . \tag{5.1}$$

In the special case $\alpha = 1/2$, we note that $(F_{1/2})^2$ is the fidelity of states [1].

Let us consider a situation illustrated in Fig. 5.1. The unitary coupling U between S and E is fixed but in 5.1 a) and b) the initial states of E and S can be different. Thus, different choices of states ξ_1 and ξ_2 of E induce channels Φ_1 and Φ_2 to S in the interaction, respectively. By exploiting the properties of the quantum Rényi divergence, defined as [103, 104]

$$S_\alpha(\rho_1||\rho_2) := \begin{cases} \dfrac{1}{\alpha-1}\ln\left\{\mathrm{tr}\left[\left(\rho_2^{\frac{1-\alpha}{2\alpha}}\,\rho_1\rho_2^{\frac{1-\alpha}{2\alpha}}\right)^\alpha\right]\right\} & \text{when } \rho_1 \not\perp \rho_2 \\ \infty & \text{otherwise} \end{cases} , \tag{5.2}$$

and the monotonicity of the logarithm function, we get

$$F_\alpha(\rho_1, \rho_2)F_\alpha(\xi_1, \xi_2) \leq F_\alpha(\Phi_1(\rho_1), \Phi_2(\rho_2)) , \tag{5.3}$$

[1] Actually, both $(F_{1/2})^2$ and $F_{1/2}$ are commonly used as fidelity of states.

for $\alpha \in [1/2, 1)$. It is worth noting that Eq. (5.3) does not explicitly depend on the coupling U, which makes it useful for different applications. Equation (5.3) can be interpreted as a generalization of the data processing inequality $F_\alpha(\rho_1, \rho_2) \leq F_\alpha(\Phi(\rho_1), \Phi(\rho_2))$, for $\alpha \in [1/2, 1)$. Motivated by this inequality, we now define the *α-fidelity of channels* Φ_1 and Φ_2 for $\alpha \in (0, 1)$ as

$$\mathcal{F}_\alpha(\Phi_1, \Phi_2) := \inf_{\rho_1, \rho_2 \in \mathcal{S}(\mathcal{H})} \frac{F_\alpha\big(\Phi_1(\rho_1), \Phi_2(\rho_2)\big)}{F_\alpha\big(\rho_1, \rho_2\big)} \,. \tag{5.4}$$

The name is justified, since $\mathcal{F}_\alpha$ shares many essential properties of the fidelity. For all $\alpha \in (0, 1)$ and channels Φ_1, $\Phi_2 : \mathcal{S}(\mathcal{H}^S) \to \mathcal{S}(\mathcal{H}^S)$, α-fidelity of channels $\mathcal{F}_\alpha(\Phi_1, \Phi_2)$ has the following properties:

$$\begin{aligned} &\mathcal{F}_\alpha(\Phi_1, \Phi_2) \in [0, 1] \,, \\ &\mathcal{F}_\alpha(\Phi_1, \Phi_2) = \mathcal{F}_\alpha(\mathcal{U} \circ \Phi_1 \circ \mathcal{V}, \mathcal{U} \circ \Phi_2 \circ \mathcal{V}) \,, \text{ for all unitary channels } \mathcal{U} \text{ and } \mathcal{V} \,. \end{aligned} \tag{5.5}$$

Additionally, for $\alpha \in [1/2, 1)$,

$$\begin{aligned} &\mathcal{F}_\alpha(\Phi_1, \Phi_2) = 1 \iff \Phi_1 = \Phi_2 \,, \\ &\mathcal{F}_\alpha(\Phi_1, \Phi_2) \leq \mathcal{F}_\alpha(\Phi \circ \Phi_1, \Phi \circ \Phi_2), \text{ for all channels } \Phi : \mathcal{S}(\mathcal{H}^S) \to \mathcal{S}(\mathcal{H}) \,, \\ &\mathcal{F}_\alpha(\Phi_1, \Phi_2) \leq \mathcal{F}_\alpha(\Phi_1 \circ \Phi, \Phi_2 \circ \Phi), \text{ for all channels } \Phi : \mathcal{S}(\mathcal{H}) \to \mathcal{S}(\mathcal{H}^S) \,. \end{aligned} \tag{5.6}$$

5.1.1 Quantum probing

Commonly, probing protocols depend on complete information of the coupling U. Here, we will show that Eq. (5.3) allows us to obtain information of ξ in quantum probing measurement with no assumption of the coupling. Such protocols can be constructed in the following way: Assume that E is prepared in the state $\xi(x, y)$ and our task is to evaluate the value of parameter x, and y is some other parameter. The experimenter has control over the initial state of S and the parameter y. By preparing S in some states ρ_1 and ρ_2 which are known, and evolving them with the channels Φ_1 and Φ_2, induced by states $\xi(x, y_1)$ and $\xi(x, y_2)$ of E, respectively, the experimenter obtains the values of $F_\alpha(\rho_1, \rho_2)$ and $F_\alpha\big(\Phi_1(\rho_1), \Phi_2(\rho_2)\big)$. When the x and y dependence of $\xi(x, y)$ is known, different values of x can be tested

in $F_\alpha(\xi(x,y_1),\xi(x,y_2))$. The values of x which cause violation of Eq. (5.3) are immediately known to be incorrect and bounds of the actual x can be obtained.

For an illustrative example, let us consider E initially in two thermal states $\xi(\beta_1)$ and $\xi(\beta_2)$ with inverse temperatures $\beta_1 = (k_B T_1)^{-1}$, and $\beta_2 = (k_B T_2)^{-1}$,

$$\xi(\beta_i) = \exp(-\beta_i H^E)/Z(\beta_i, H^E)\,, \text{ for } i \in \{1,2\}\,. \tag{5.7}$$

Here, H^E is some Hamiltonian of E and $Z(\beta_i, H_E) := \mathrm{tr}[\exp(-\beta_i H_E)]$ is the corresponding partition function for $i \in \{1,2\}$. The goal is to gain information on some parameters of environment Hamiltonian H^E. By using Eq. (5.3) in this situation, we get

$$\ln\left[\frac{Z(\alpha\beta_1+(1-\alpha)\beta_2, H^E)}{Z(\beta_1,H^E)^\alpha Z(\beta_2,H^E)^{(1-\alpha)}}\right] \leq \inf_{t\geq 0}\begin{cases} \ln[\mathcal{F}_\alpha(\Phi_2^{(t)},\Phi_1^{(t)})], \text{ for } \alpha\in(0,\frac{1}{2}) \\ \ln[\mathcal{F}_\alpha(\Phi_1^{(t)},\Phi_2^{(t)})], \text{ for } \alpha\in[\frac{1}{2},1) \end{cases}, \tag{5.8}$$

where we have exploited the commutativity of the thermal states to extend α to cover the whole interval $(0,1)$.

We assume that the experimenter has control over temperatures β_1 and β_2 of E. The values of $\mathcal{F}_\alpha$ in the right-hand side of Eq. (5.8) can be obtained from tomographical measurements on the evolved states $\Phi_1(\rho_1)$ and $\Phi_2(\rho_2)$ of S. Making a hypothesis about H^E determines the left-hand side of the inequality. If the inequality is violated, the hypothesis of H^E can be ruled out as incompatible with the induced pair of dynamics, without any information of the coupling between S and E.

We further specify the example by fixing S as a qubit coupled to E which is a single harmonic oscillator. This corresponds to a two-level atom passing through an optical cavity with a single electromagnetic quantized mode. Assume that $H^E = \omega(b^\dagger b + \frac{1}{2}\mathbb{1})$, the coupling is unknown, and the parameter to be determined is the oscillator frequency ω. By fixing β_1 and β_2 and choosing different values for ω we plot the dashed coloured curves in Fig. 5.2 corresponding to the left-hand side of Eq. (5.8).

To simulate the measurement data on the right-hand-side of Eq. (5.8) corresponding to the black curve in Fig. 5.2, we consider the total Hamil-

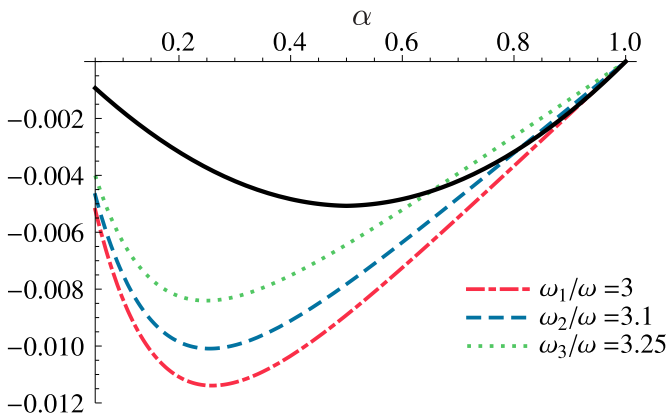

Figure 5.2: A Harmonic oscillator is prepared in thermal states with temperatures $T_1 = 0.25\omega$ and $T_2 = 0.75\omega$. The dynamics of S gives the right-hand-side of Eq. (5.8), illustrated by the black curve. The three colored curves correspond to the left-hand-side of Eq. (5.8) for guesses ω_1, ω_2, and ω_3 for the oscillator frequency ω. The choice $\omega_1/\omega = 3$ satisfies Eq. (5.8) while the other guesses violate it. The initial states of S are $\rho_1 = \rho_2 = |+\rangle\langle+|$, where $|+\rangle = \frac{1}{\sqrt{2}}(|0\rangle + |1\rangle)$.

tonian

$$H = H^S + H^E + H^I = \frac{\omega_0}{2}\sigma_3 + \omega\left(b^\dagger b + \frac{1}{2}\mathbb{1}\right) + \sigma_3 \otimes \left(gb^\dagger + g^* b\right) \quad (5.9)$$

which is unknown to the experimenter[2]. We see from Fig. 5.2 that the inequality forbids any frequency values greater than 3.1 times the real frequency ω. We also note that none of the colored lines crosses the black line for $\alpha \leq 0.5$. When α increases beyond 0.65, we see that the green line crosses the black line, implying that it cannot correspond to the correct value of ω. Further increasing α above 0.8 shows that the frequency corresponding to the blue line is also incorrect. This serves as evidence on how the freedom in choosing α can lead to increased precision.

[2]The dynamics for S, induced by the Hamiltonian in Eq. (5.9), is presented in [37].

5.1.2 Limitations of reservoir engineering of pure dephasing dynamics

The α-fidelity of the initial environmental states can reveal certain properties of unsolvable induced dynamics, such as coherence trapping and non-Markovianity in the sense of revivals of trace distance. We concentrate on one-qubit dephasing channels arising from interaction between the qubit and its environment. Pure dephasing is a special case of phase covariant dynamics where $\gamma_1(t) = \gamma_2(t) = 0$ and it can be written in the matrix representation as

$$\Phi_t(\rho(0)) = \rho(t) = \begin{pmatrix} \rho_{00} & D^*(t)\rho_{01} \\ D(t)\rho_{10} & \rho_{11} \end{pmatrix}, \tag{5.10}$$

where $D(t) = \exp\left[\int_0^t i2\omega(\tau) - \gamma_3(\tau)\right]$ is the so-called *decoherence function*.

Let $D_1(t)$ and $D_2(t)$ be the decoherence functions induced by the environment in states ξ_1 and ξ_2, respectively. If the system is initially in state $\rho_1(0) = \rho_2(0) = |+\rangle\langle+|$, choosing $\alpha = 1/2$ in Eq. (5.3) gives

$$\begin{aligned} F_{1/2}(\xi_1, \xi_2) \leq & \frac{1}{2}\left[\sqrt{(1 - D_1(t))(1 - D_2(t))}\right. \\ & \left. + \sqrt{(1 + D_1(t))(1 + D_2(t))}\right], \end{aligned} \tag{5.11}$$

If ξ_1 and $D_1(t)$ are known, upper and lower bounds for $D_2(t)$ corresponding to any ξ_2 can be solved from Eq. (5.11). Thus, the variety of pure dephasing dynamics induced by ξ_2 is limited by $D_1(t)$ and the fidelity between ξ_1 and ξ_2. On the other hand, these limitations let us make useful conclusions on the characteristic properties of $D_2(t)$ without solving it directly.

Let us consider an example case where the analytical solution for the qubit dynamics, given by $D_1(t)$, is known only for some initial states ξ_1 of the environment, namely a qubit coupled to an Ising chain in a transverse field. The evolution of the total system is governed by the Hamiltonian

$$H(J, \lambda, \delta) = -J \sum_j \left(\sigma_3^j \sigma_3^{j+1} + \lambda\, \sigma_1^j + \delta\, |e\rangle\langle e| \sigma_1^j\right), \tag{5.12}$$

where J, λ, and δ are the strength of the nearest neighbour coupling in the Ising chain, its coupling to the transverse field, and the qubit–chain

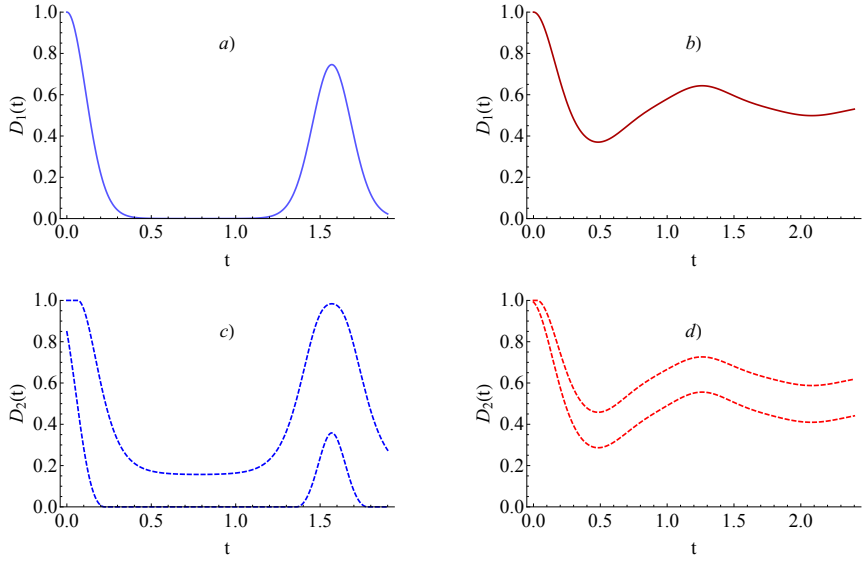

Figure 5.3: a) and b): The dynamics of the decoherence function induced by the ground state ξ_1 of the environment Hamiltonian for a) $\lambda = 0.01$, and b) $\lambda = 1.8$. Here we have chosen $J = 1$, $\delta = 0.1$, and $N = 4000$. c) and d): The bounds of the unknown decoherence function for c) $\lambda = 0.01$, $F_{1/2}(\xi_1, \xi_2) = 0.98$, and d) $\lambda = 1.8$, $F_{1/2}(\xi_1, \xi_2) = 0.999$.

coupling, respectively [105, 106]. It is known, that a pure initial state of the Ising chain results to pure dephasing dynamics of the qubit. When ξ_1 is chosen as the ground state of the environmental Hamiltonian, the decoherence function of the qubit can be solved as

$$D(\lambda, t) = \Pi_{k>0}(1 - \sin^2(2\alpha_k)\sin^2(\varepsilon_k t)) \,, \tag{5.13}$$

where, ϵ_k and α_k are the single quasiexcitation energies, and Bogoliubov angles, respectively. Both of these depend on λ, and thus changing λ affects the dynamics [105, 106]. In the following, we fix the number of spins in Ising chain to 4000 and use $J = 1$ and $\delta = 0.1$.

Equation (5.11) gives an estimate for the decoherence function $D_2(t)$ for any other pure initial state ξ_2 of the Ising chain. In Fig. 5.3 a) and b), we present the qubit dynamics induced by the Ising chain in the ground state for $\lambda = 0.01$ and $\lambda = 1.8$, respectively. In Fig. 5.3 c) and d), we present

the upper and lower bounds for the unknown solutions, analytically solved by using a) and b), respectively. We note that the lower bounds increase above the first local minimum of the upper bound. This implies guaranteed revivals in the decoherence function and thus information back flow in the sense of increasing trace distance[3]. In Fig. 5.3 d), we see that also the coherence trapping property can be guaranteed if the inducing state of the Ising chain is chosen close enough to the ground state of the chain Hamiltonian for $\lambda = 1.8$.

5.2 Solving fidelity membership problems

In the quantum probing protocols we proposed, the only quantity that has to be experimentally determined was the α-fidelity of the evolved states $\Phi_1(\rho_1)$ and $\Phi_2(\rho_2)$. Commonly, this is obtained by performing full tomography but if it has to be done for multiple initial state pairs and pairs of environment's control parameters, the process becomes quickly very demanding. In this section, we propose and experimentally implement a protocol which allows us to both evaluate upper and lower bounds for the fidelity between two states and solve so-called membership problems without resorting to full tomography.

For a more abstract problem, let us consider a partition of the state space $\mathcal{S}(\mathcal{H})$ into disjoint subsets $\mathcal{P}_k$ of $\mathcal{S}(\mathcal{H})$ such that $\mathcal{S}(\mathcal{H}) = \cup_k \mathcal{P}_k$. *Membership problem* is a task of determining conclusively, which of the segments $\mathcal{P}_k$ contains the unknown state ρ [107]. Even though informationally complete measurements can solve any membership problem, they should be avoided, if possible: since the number of parameters to be determined in tomography increases as d^2, it becomes experimentally too demanding and time-consuming for high-dimensional systems. It is also of foundational interest to understand which membership problems can be solved with an informationally incomplete measurement. Recently, the necessity of informationally complete POVM's in various membership problems has been studied [64, 107, 108]. We will concentrate on the fidelity membership problem and solve it experimentally in a two-photon polarization system with informationally incomplete measurement.

[3] Actually, this holds for all of the memory effects studied in this thesis, since in the case of $\gamma_1(t) = \gamma_2(t) = 0$, meaning pure dephasing, increasing $D(t)$ is equivalent to $\gamma_3(t) < 0$.

5.2.1 Fidelity membership problem

Let us start by fixing a boundary state σ. We use the fidelity between the *reference state* σ and the unknown state to form the following membership problem: The task is to determine, whether the unknown state is at least as close to σ as some boundary value ϵ with respect to fidelity or not. In other words, we want to find in which part of the state space partition $\mathcal{S}(\mathcal{H}) = \mathcal{S}_\sigma^{\geq\epsilon} \cup \mathcal{S}_\sigma^{<\epsilon}$ the unknown state is. Here, we have denoted

$$\mathcal{S}_\sigma^{\geq\epsilon} = \{\rho \in \mathcal{S}(\mathcal{H}) : F(\rho,\sigma) \geq \epsilon\}\,, \quad \mathcal{S}_\sigma^{<\epsilon} = \{\rho \in \mathcal{S}(\mathcal{H}) : F(\rho,\sigma) < \epsilon\} \tag{5.14}$$

for any $\epsilon \in [0,1]$. Let E be a POVM with the set of so-called perturbation operators Δ, defined as

$$\mathcal{X}_E := \{\Delta \in \mathcal{L}(\mathcal{H}) : \mathrm{tr}[\Delta E_j] = 0\ \forall j,\ \mathrm{tr}[\Delta] = 0,\ \Delta^\dagger = \Delta\}\,. \tag{5.15}$$

The fidelity membership problem can be solved conclusively by measuring the POVM E with perturbations Δ satisfying [107]

$$\sqrt{\sigma}\Delta\sqrt{\sigma} = 0\,. \tag{5.16}$$

Here, solving the membership problem conclusively means that for any state $\rho \in \mathcal{S}(\mathcal{H})$ the measurement outcome distribution can be analyzed to reveal that ρ belongs exclusively to $\mathcal{S}_\sigma^{\geq\epsilon}$ or $\mathcal{S}_\sigma^{<\epsilon}$. On the other hand, violation of Eq. (5.16) by any perturbation $\Delta \in \mathcal{X}_{E'}$ of POVM E', implies that there exists at least one pair of states $\rho_1 \in \mathcal{S}_\sigma^{\geq\epsilon}$ and $\rho_2 \in \mathcal{S}_\sigma^{<\epsilon}$ such that measuring E' on them results to exactly the same outcome probability distribution.

The number of segments in the membership problem can be increased by using simultaneously multiple reference states. For example, using two reference states, χ and ξ, and fixing their corresponding fidelity boundary values, α and β, we can form the four segmented partition of the state space:

$$\mathcal{S}(\mathcal{H}) = \mathcal{P}_1 \cup \mathcal{P}_2 \cup \mathcal{P}_3 \cup \mathcal{P}_4\,, \quad \text{where} \tag{5.17}$$

$$\begin{aligned} &\mathcal{P}_1 = \mathcal{S}_\chi^{<\alpha} \cap \mathcal{S}_\xi^{\geq\beta}\,,\ \mathcal{P}_2 = \mathcal{S}_\chi^{\geq\alpha} \cap \mathcal{S}_\xi^{\geq\beta}\,, \\ &\mathcal{P}_3 = \mathcal{S}_\chi^{<\alpha} \cap \mathcal{S}_\xi^{<\beta}\,,\ \mathcal{P}_4 = \mathcal{S}_\chi^{\geq\alpha} \cap \mathcal{S}_\xi^{<\beta}\,. \end{aligned} \tag{5.18}$$

In order to solve the extended membership problem in Eq. (5.17), the POVM E now has to satisfy the condition of Eq. (5.16) for both $\sigma = \chi$ and

$\sigma = \xi$.

For any pure reference state $\sigma = |\varphi_\sigma\rangle\langle\varphi_\sigma|$, there exists a POVM with only two elements, namely $E_1 = \sigma$, $E_2 = \mathbb{I} - \sigma$, which solves the fidelity membership problem. Now, the definition of the perturbations gives

$$0 = \mathrm{tr}[\Delta E_1] = \langle\varphi_\sigma|\Delta|\varphi_\sigma\rangle\,. \tag{5.19}$$

In this case, the left-hand side of Eq. (5.16) becomes

$$|\varphi_\sigma\rangle\langle\varphi_\sigma|\Delta|\varphi_\sigma\rangle\langle\varphi_\sigma| = 0\,, \tag{5.20}$$

which shows that each $\Delta \in \mathcal{X}_E$ satisfies Eq. (5.16).

Unfortunately, the projections on all entangled pure states cannot be performed with simultaneous local measurements on the subsystems of multi-partite systems. We will show how the fidelity membership problem of maximally entangled reference states can be experimentally solved with informationally incomplete set of simultaneous local projections.

We restrict to the two-qubit cases where σ is one of the Bell states $|\Psi^-\rangle = \frac{1}{\sqrt{2}}(|01\rangle - |10\rangle)$ or $|\Psi^+\rangle = \frac{1}{\sqrt{2}}(|01\rangle + |10\rangle)$ and form the following four segmented partition of the state space:

$$\mathcal{S}(\mathcal{H}) = \mathcal{P}_1 \cup \mathcal{P}_2 \cup \mathcal{P}_3 \cup \mathcal{P}_4\,, \qquad \text{where} \tag{5.21}$$

$$\begin{aligned} \mathcal{P}_1 &= \mathcal{S}_{\Psi^-}^{<\epsilon^-} \cap \mathcal{S}_{\Psi^+}^{\geq\epsilon^+}\,,\ \mathcal{P}_2 = \mathcal{S}_{\Psi^-}^{\geq\epsilon^-} \cap \mathcal{S}_{\Psi^+}^{\geq\epsilon^+}\,, \\ \mathcal{P}_3 &= \mathcal{S}_{\Psi^-}^{<\epsilon^-} \cap \mathcal{S}_{\Psi^+}^{<\epsilon^+}\,,\ \mathcal{P}_4 = \mathcal{S}_{\Psi^-}^{\geq\epsilon^-} \cap \mathcal{S}_{\Psi^+}^{<\epsilon^+}\,. \end{aligned} \tag{5.22}$$

Measuring E solves simultaneously the fidelity membership problem with respect to Ψ^- and Ψ^+ if and only if

$$\langle 01|\Delta|01\rangle + \langle 10|\Delta|10\rangle = \mathrm{Re}\,(\langle 01|\Delta|10\rangle) = 0 \quad \forall\,\Delta \in \mathcal{X}_E\,. \tag{5.23}$$

5.2.2 The experimental setup

We solve the fidelity membership problem for the polarization states of two photons. We fix the matrix representation as $|H\rangle = (1\ 0)^{\mathrm{T}}, |V\rangle = (0\ 1)^{\mathrm{T}}$. In the experiment, a pair of photons in polarization entangled state $|\Psi^-\rangle = \frac{1}{\sqrt{2}}(|HV\rangle - |VH\rangle)$ is produced in a parametric down-conversion process. Each of the photons is coupled to a single mode optical fiber and guided into its respective detection station, illustrated in Fig. 5.4.

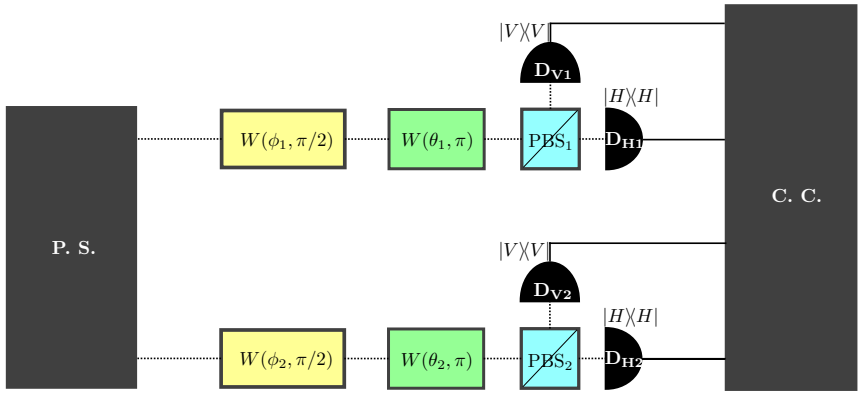

Figure 5.4: The experimental setup for performing local projective measurements on the polarization states of photons 1 and 2. Here $k \in \{1, 2\}$ labels the photon and $i \in \{H, V\}$ is the polarization in the laboratory coordinates. P. S. – the photon source which produces the unknown 2 photon polarization states. $W(\phi_k, \pi/2)$ – quarter-wave plates and $W(\theta_k, \pi)$ – half-wave plates which rotate the measurement bases. PBS$_k$ – polarizing beam splitters and D_{ik} – single-photon detectors which perform the projective measurements on the rotated bases. C. C. – the coincidence counting electronics which collects the statistics of the coincidences of photon detections.

In the detection stations, the bases of projective measurements on the polarization qubits are rotated with half-wave plates $W(\theta_k, \pi)$ and quarter-wave plates $W(\phi_k, \pi/2)$, where $k \in \{1, 2\}$. In the fixed matrix representation, the action of a wave plate on the one-photon polarization state ρ can be written as $W(\mu, \nu)\rho W(\mu, \nu)^\dagger$, where

$$W(\mu, \nu) = \begin{pmatrix} \cos^2(\mu) + e^{i\nu}\sin^2(\mu) & \frac{1}{2}(1 - e^{i\nu})\sin(2\mu) \\ \frac{1}{2}(1 - e^{-i\nu})\sin(2\mu) & \sin^2(\mu) + e^{i\nu}\cos^2(\mu) \end{pmatrix} \tag{5.24}$$

and μ and ν correspond to rotation angle and phase shift of the wave plate, respectively. This means that the total two-qubit measurement bases can

be rotated with operators

$$\begin{aligned} A_{1,2}(\theta_1, \phi_1, \theta_2, \phi_2) &:= A_1(\theta_1, \phi_1) \otimes A_2(\theta_2, \phi_2), \quad \text{where} \\ A_k(\theta_k, \phi_k) &:= W(\phi_k, \pi/2)^\dagger W(\theta_k, \pi)^\dagger, \quad \text{and}\, k \in \{1, 2\}\,. \end{aligned} \tag{5.25}$$

After the wave plate rotations, the projections on the measurement basis elements, corresponding to our POVM elements, are

$$\begin{aligned} &P_{i,j}(\theta_1, \phi_1, \theta_2, \phi_2) \\ &:= A_{1,2}(\theta_1, \phi_1, \theta_2, \phi_2)|i\rangle\langle i| \otimes |j\rangle\langle j|A^\dagger_{1,2}(\theta_1, \phi_1, \theta_2, \phi_2)\,,\ i, j \in \{H, V\}\,. \end{aligned} \tag{5.26}$$

Finally, each photon goes through a polarizing beam splitter PBS_k and ends up at a detector D_{Vk} or D_{Hk}. For each rotated polarization basis, the measurement data consists of coincidence counts in detector combinations

$$\{(H1, H2), (H1, V2), (V1, H2), (V1, V2)\}\,. \tag{5.27}$$

5.2.3 POVM to solve the fidelity membership problem

In Table 5.1, we present three combinations of wave plate rotation angles, corresponding to projective measurements on the elements of the orthonormal bases, $\mathcal{B}_1$, $\mathcal{B}_2$ and $\mathcal{B}_3$, used in the experiment. For each basis, the measurement is repeated for multiple identical copies of the unknown state and the probability distribution of the measurement outcomes is collected. In the measurement, the total set of POVM elements is $E = \frac{1}{3}\mathcal{B}_1 \cup \frac{1}{3}\mathcal{B}_2 \cup \frac{1}{3}\mathcal{B}_3$. Since the dimension of E is 10, and the POVM is informationally complete if and only if $\dim(E) = d^2 = 16$, we conclude that E is informationally incomplete.

Equation (5.23) shows that E solves the four segmented membership problem of Eq. (5.21). We note that also choices $\sigma = |\varphi_\sigma\rangle\langle\varphi_\sigma|$, where $|\varphi_\sigma\rangle = |00\rangle$, $|\varphi_\sigma\rangle = |01\rangle$, $|\varphi_\sigma\rangle = |10\rangle$, $|\varphi_\sigma\rangle = |11\rangle$, $|\varphi_\sigma\rangle = \frac{1}{\sqrt{2}}(|00\rangle - |11\rangle)$, and $|\varphi_\sigma\rangle = \frac{1}{\sqrt{2}}(|00\rangle + |11\rangle)$, satisfy the condition of Eq. (5.16). Thus, all these reference states can be used to form a 2^8 partite membership problem which our POVM E solves.

Keeping, the bases $\mathcal{B}_1$ and $\mathcal{B}_2$ the same as in Table 5.1 and replacing $\mathcal{B}_3$ by seven other bases, one can construct another POVM whose dimension is

Table 5.1: Three orthonormal bases, $\mathcal{B}_1$, $\mathcal{B}_2$ and $\mathcal{B}_3$, forming a sufficient set of projective measurements to solve the fidelity membership problem with respect to Ψ^- and Ψ^+. Here θ_k and ϕ_k are the rotation angles of half-wave plate and quarter-wave plate of photon $k \in \{1, 2\}$, respectively.

	$\mathcal{B}_1$	$\mathcal{B}_2$	$\mathcal{B}_3$
ϕ_1	0	$\pi/4$	0
θ_1	0	$\pi/8$	$\pi/8$
ϕ_2	0	$\pi/4$	0
θ_2	0	$\pi/8$	$\pi/8$

13, but is incapable of solving the membership problem. This serves as an example of how higher dimension of the POVM does not necessarily mean that it is more capable of solving a given membership problem.

5.2.4 Measurement results

We solved the membership problem in the experiment for two unknown states, Preparation 1 and Preparation 2, which were prepared close to the states Ψ^- and Ψ^+, respectively. The measured probability distributions of the three bases are combined into a normalized vector $\mathbf{p}$. The SLSQP optimization algorithm in the Python method `scipy.optimize.minimize` solves numerically the density matrix $\rho(\mathbf{b})$, whose measurement outcome distribution is closest to the distribution in the experiment. The density matrix is parametrized with the generalized Bloch vector $\mathbf{b} \in \mathbb{R}^{15}$ as $\rho(\mathbf{b}) = \frac{1}{4}\mathbb{I} + \mathbf{b}\cdot\mathbf{\Gamma}$, where Γ_i are the 4×4 generalizations of Gell-Mann matrices [109].

The vector $\mathbf{b}$ is used as the optimization parameter and the ℓ_1-distance $d_1(\mathbf{p}, \mathbf{q}) = \sum_i |p_i - q_i|$ is minimized. Here, p_i is the probability of outcome e_i in the experiment, and $q_i = \mathrm{tr}[E_i\rho(\mathbf{b})]$. The positivity of $\rho(\mathbf{b})$ is guaranteed by using the positivity of its eigenvalues as optimization constraint. Applying the constraint $\rho(\mathbf{b}) \in \mathcal{P}_k$ in SLSQP guarantees that $d_1(\mathbf{p}, \mathbf{q}) = 0$ if and only if $\rho \in \mathcal{P}_k$ for the unknown state ρ in the experiment.

In Fig. 5.5, we present the results for two unknown state preparations in the experiment. For both preparations, we show the solution to the fidelity membership problem for four different partitions. The difference between

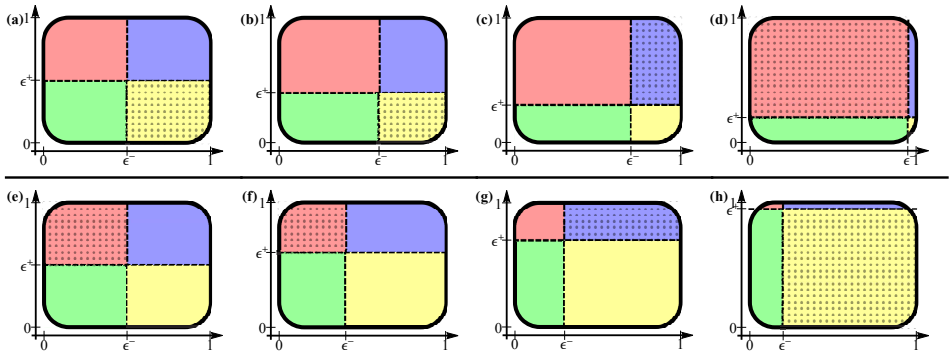

Figure 5.5: **The analysis of the membership problems (a) – (d):** for Preparation 1. **(e) – (h):** for Preparation 2. For both preparations, the boundary fidelity values, ϵ^- and ϵ^+, with respect to the reference states Ψ^- and Ψ^+, are changed to form a different partition in each panel. Fixing the values of ϵ^- and ϵ^+ forms a partition of the state space into four disjoint segments. Here, ϵ^- and ϵ^+ correspond to the vertical and horizontal dashed lines, respectively, and the disjoint segments are illustrated with different colors. For each partition, exactly one of the segments contains the numerically determined optimal density operator $\rho(\mathbf{b})$ whose outcome distribution is the same as in the experiment. The segment which contains the unknown sate is marked by dotting. **(a)** $\epsilon^- = \sqrt{0.5}$, $\epsilon^+ = \sqrt{0.5}$, **(b)** $\epsilon^- = \sqrt{0.6}$, $\epsilon^+ = \sqrt{0.4}$, **(c)** $\epsilon^- = \sqrt{0.7}$, $\epsilon^+ = \sqrt{0.3}$, **(d)** $\epsilon^- = \sqrt{0.95}$, $\epsilon^+ = \sqrt{0.2}$. **(e)** $\epsilon^- = \sqrt{0.5}$, $\epsilon^+ = \sqrt{0.5}$, **(f)** $\epsilon^- = \sqrt{0.4}$, $\epsilon^+ = \sqrt{0.6}$, **(g)** $\epsilon^- = \sqrt{0.3}$, $\epsilon^+ = \sqrt{0.7}$, **(h)** $\epsilon^- = \sqrt{0.2}$, $\epsilon^+ = \sqrt{0.95}$.

the partitions is the values of the fidelity boundaries ϵ^- and ϵ^+, illustrated by the vertical and horizontal dashed lines, respectively. The area to the right and left from the vertical dashed line at ϵ^-, are the sets $\mathcal{S}_{\Psi^-}^{\geq\epsilon^-}$ and $\mathcal{S}_{\Psi^-}^{<\epsilon^-}$, respectively. The areas above and below the horizontal dashed line at ϵ^+, are the sets $\mathcal{S}_{\Psi^+}^{\geq\epsilon^+}$ and $\mathcal{S}_{\Psi^+}^{<\epsilon^+}$, respectively. The dotted area denotes the unique segment of the partition which contains the unknown state.

In each partition and for both state preparations in the experiment, we find that in exactly one of the segments the optimal density operator $\rho(\mathbf{b})$ produces the same outcome distribution as measured. Thus, each membership problem was conclusively solved. Our result serves also as

experimental evidence for the effectiveness of the geometric approach of [64] in solving membership problems. The result of [107] can be easily be generalized to α-fidelities by replacing $\sqrt{\rho}$ with $\rho^{\frac{1-\alpha}{2\alpha}}$ in Eq. (5.16). Thus, the method can be used to obtain upper and lower bounds for the α-fidelities of evolved states required in our proposed quantum probing protocol.

5.3 Fully-controllable dephasing dynamics

Previously, we saw what kind of restrictions the known solution of the decoherence function $D_1(t)$, induced by environment in state ξ_1, and the α-fidelity between ξ_1 and ξ_2 impose on the decoherence function $D_2(t)$, induced by environment state ξ_2 when the system and environment are initially uncorrelated. Now, we go beyond the assumption of uncorrelated initial states. We show how exploiting the initial correlations between system and environment gives us full control over the dynamics described by pure dephasing channels Φ_t:

$$\Phi_t(\rho(0)) = \rho(t) = \begin{pmatrix} \rho_{00} & D^*(t)\rho_{01} \\ D(t)\rho_{10} & \rho_{11} \end{pmatrix}, \tag{5.28}$$

We choose the polarization of a photon as the open system and the frequency degree of freedom of the same photon as the environment. One and two-photon polarization has been recently used to study open system dynamics and memory effects [51, 56, 57, 65, 93, 110, 111]. We start with a pure initial polarization-frequency state for the photon

$$|\Psi\rangle = C_V|V\rangle \int g(\omega)|\omega\rangle d\omega + C_H|H\rangle \int e^{i\theta(\omega)} g(\omega)|\omega\rangle d\omega. \tag{5.29}$$

Here V and H correspond to vertical and horizontal polarizations with amplitudes C_V and C_H, respectively. ω are the frequency values with amplitude $g(\omega)$, and $\theta(\omega)$ is the frequency dependent phase factor for H polarization. The state is normalized with $|C_H|^2 + |C_V|^2 = 1$ and $\int |g(\omega)|^2 d\omega = 1$.

Once the coupling $U(t)$ is fixed, the total initial polarization-frequency state dictates the polarization dynamics completely, as described by Eq. (2.5). Polarization and frequency are coupled in birefringent medium, such as

quartz or calcite. The coupling Hamiltonian is [110]

$$H = \frac{1}{\hbar}(n_H|H\rangle\langle H| + n_V|V\rangle\langle V|)\int 2\pi\omega|\omega\rangle\langle\omega|d\omega, \tag{5.30}$$

where n_H and n_V are the refractive indices of the medium in the H and V directions, respectively. By tracing out the frequency degree of freedom, the reduced polarization dynamics becomes

$$\begin{aligned}\rho(t) &= \begin{pmatrix} |C_H|^2 & \kappa^*(t)C_H C_V^* \\ \kappa(t)C_V C_H^* & |C_V|^2 \end{pmatrix}, \quad \text{where} \\ \kappa(t) &= \int |g(\omega)|^2 e^{i\theta(\omega)} e^{i2\pi\Delta n\omega t} d\omega\,,\end{aligned} \tag{5.31}$$

$\Delta n = n_H - n_V$ and t is the interaction time. We note that $\kappa(t)$ is independent of the choice of the initial state, and the map is linear. Thus the dynamics of mixed polarization states is also given by Eq. (5.31).

Equation (5.31) reveals that $\kappa(t)$ is the Fourier transformation of the distribution $|g(\omega)|^2 e^{i\theta(\omega)}$. Since Fourier transform is invertible, this connection tells directly how the distributions $g(\omega)$ and $\theta(\omega)$ should be chosen to induce any desired polarization dephasing dynamics defined by any complex function $\kappa(t)$. On the other hand, for each $\kappa(t)$ the corresponding complex distribution $|g(\omega)|^2 e^{i\theta(\omega)}$ is unique, and thus implementing non-trivial $\theta(\omega)$'s is necessary for full freedom of choosing the dephasing dynamics. Since the normalization condition $\int |g(\omega)|^2 d\omega = 1$ has to be satisfied, implementing any non-trivial phase distribution $\theta(\omega)$ implies $|\kappa(0)| < 1$. We note from Eq. (5.31) that if $|\kappa(0)| < 1$, the initial polarization state is not pure, unless $C_V = 0$ or $C_H = 0$.

For the evolved total state, the entropy of entanglement between polarization and frequency becomes

$$E\left(U(t)|\Psi\rangle\langle\Psi|U(t)^\dagger\right) = h_2\left[\frac{1+\sqrt{1+4|C_H C_V|^2(|\kappa(t)|^2-1)}}{2}\right], \tag{5.32}$$

where h_2 is the binary Shannon entropy function. Entanglement of entropy increases monotonically as the decoherence coefficient $|\kappa(t)|$ decreases. This means, that a faithful implementation of the dynamics requires delicate control of both the initial frequency and the initial correlations between the polarization and frequency.

The CP and positivity conditions for single-qubit dephasing channels in Eq. (5.28) are equivalent, namely $|D(t)| \leq |D(0)|$. However, the control over $\kappa(t)$ in our setup allows implementing non-positive dynamics: Due to initial system-environment correlations induced by non-trival distribution $\theta(\omega)$, we have cases with $|\kappa(0)| < 1$. Therefore, the full control of the dynamics and exploiting the initial system-environment correlations allows us to implement non-positive dynamics violating $|\kappa(t)| \leq |\kappa(0)|$. Even though the dynamics is non-positive, all physically implementable initial states $\rho(0)$ are still mapped into positive trace one operators, corresponding to physical states: Whenever $|\kappa(0)| < 1$, the set of all initial states $\rho(0)$ in Eq. (5.31) is shrunk towards the z axis of the Bloch ball. As these initial states evolve in time, the radius of the set in the xy plane can increase. The evolved states will still always be bounded by the original Bloch sphere, keeping them positive. On the other hand, if we apply the dynamics on a positive operator initially on the boundary of the Bloch ball, it will be mapped outside the Bloch sphere whenever $|\kappa(0)| < |\kappa(t)|$, making the dynamics non-positive.

In the experiment, a photon pair is produced in spontaneous parametric down conversion process. Each of the photons in the pair is coupled into a separate single-mode fiber. One of the photons is sent to the experimental device in Fig. 5.6, and the other is used as a trigger for data collection.

In the device, a half-wave plate (HWP) maximizes the H component and a polarizing beam splitter (PBS) filters out the V component of polarization. Another HWP rotates the polarization from $|H\rangle$ to superpositions $\frac{1}{\sqrt{2}}(|H\rangle \pm |V\rangle)$. A beam displacer directs the V component to a lower branch, allowing independent manipulation of the polarization components. Before the photon goes through three gratings, $|V\rangle$ is rotated to $|H\rangle$ by the HWP core of the composite component GCHWP. This bypasses errors caused by the polarization dependency of the grating efficiency and the ability of the SLM to modulate only the H polarization.

Then the photon is diffracted in the horizontal direction with gratings. This converts the frequency modes into spatial modes. A collimating lens (PCCL) parallelizes the spatial modes which proceed to the spatial light modulator (SLM). The SLM can introduce complex phase differences between the spatial modes and manipulate the reflected intensity distribution of the frequency. These manipulations can be performed independently for the upper and lower branches.

From the SLM the photon is reflected back through the PCCL and three

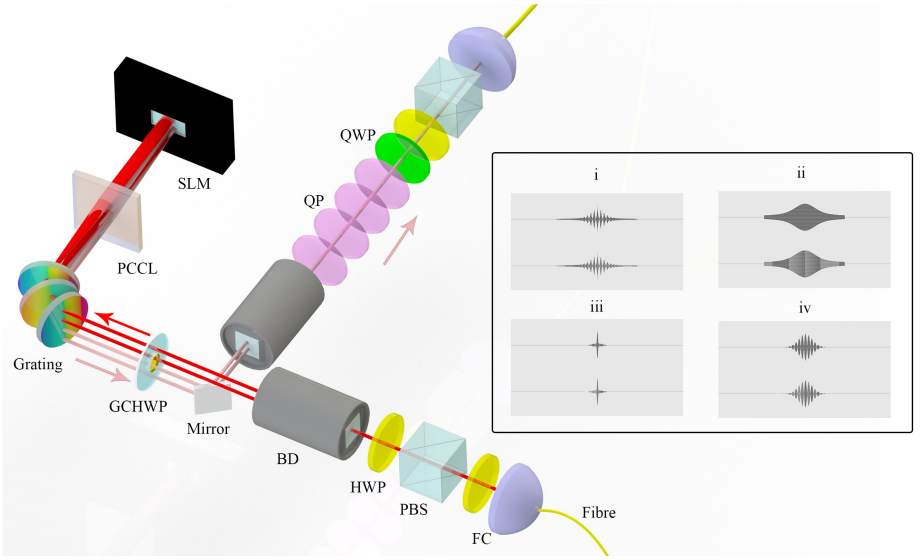

Figure 5.6: The experimental setup. FC – fiber connector, PBS – polarizing beam splitter, HWP – half-wave plate, BD – beam displacer, GCHWP– glass cemented half-wave plate, PCCL – plano convex cylindrical lense, SLM – spatial light modulator, QP – quartz plate, and QWP – quarter-wave plate. The inset shows the holograms used in the experiment so that (i) - (iv) correspond to Fig. 3 (a)-(d).

gratings, collimating and recombining the spatial modes into one mode in each branch. The branches pass through the same GCHWP rotating the polarization of the upper branch from $|H\rangle$ to $|V\rangle$. A mirror guides both branches through another BD combining them back into one. In this way, the total polarization–frequency state in the shape of Eq. (5.29) has been prepared. Controlling the reflected intensity and complex phase distributions with SLM allows us to fully control the distributions $g(\omega)$ and $\theta(\omega)$ in Eq. (5.29), respectively. Thus, the setup allows for full control of the dephasing dynamics of the polarization state as shown in Eq. (5.31).

The recombined photon passes through a combination of quartz plates (QP) which couple the polarization with frequency according to interaction Hamiltonian (5.30). The total interaction time is controlled by changing the thickness of the QP combination. For each selected interaction time

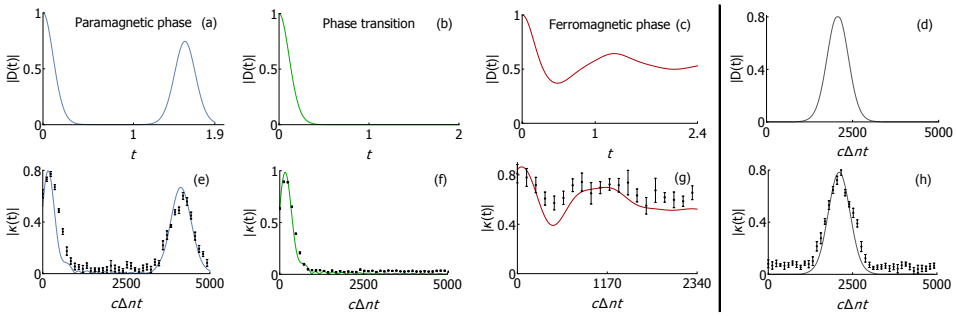

Figure 5.7: Goal dynamics and their implementation. **(a–c):** The decoherence function $D(t)$ in the qubit–Ising chain model as function of time in seconds. (a), (b), and (c) correspond to $\lambda = 0.01$, $\lambda = 0.9$, and $\lambda = 1.8$, respectively. **(d):** The dynamics of $D(t)$ for a non-positive example of dephasing. **(e–g):** Experimentally implemented dynamics of $|\kappa(t)|$ corresponding to panels (a)-(c) as function of effective path difference in units of 800 nm. The black dots correspond to measurement data. The solid curves are theoretical fits for the measurement data. **(h):** The measured dynamics of $|\kappa(t)|$ in the non-positive dynamics of panel (d). The results clearly show high control and violation of $|\kappa(t)| \leq |\kappa(0)|$.

t, a combination of a quarter-wave plate, HWP, and PBS is used to run a tomographic measurement to determine the density matrix $\rho(t)$ of the polarization qubit. In this way, we obtain the values of $|\kappa(t)|$.

For an experimental demonstration, we implement in the polarization the dynamics of a qubit interacting with Ising chain in transverse field [105, 106]. As before, we fix $J = 1$ and $\delta = 0.1$, and the number of Ising chain spins as 4000. Using different choices of λ results to very different and exotic dephasing dynamics, which makes the model a good example to test our protocol. The Ising chain ground state exhibits a quantum phase transition when $\lambda + \delta = 1$ from paramagnetic to ferromagnetic phase, and results to monotonic decay of coherences exclusively in the phase transition point. Figures 5.7(a), (b), and (c) display the dynamics of the decoherence function for parameters $\lambda = 0.01$, $\lambda = 0.9$ and $\lambda = 1.8$, corresponding to paramagnetic, phase transition point, and ferromagnetic phase, respectively. In Fig. 5.7(a) the decoherence function decreases quickly destroying the coherences which later revive almost completely indicating non-Markovianity

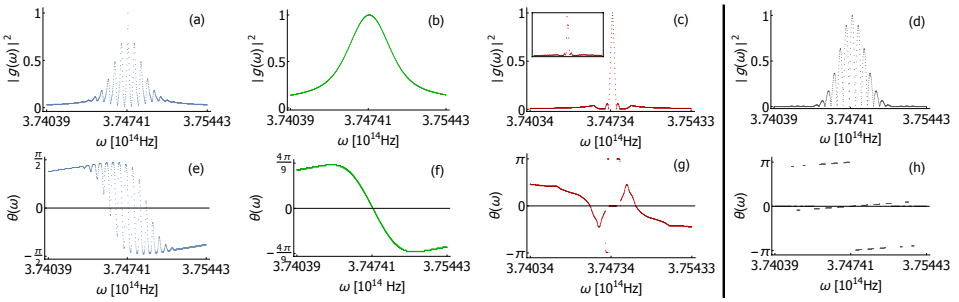

Figure 5.8: Implemented photon frequency and phase distributions. **(a-d):** Intensity distributions $|g(\omega)|^2$ of the photon frequency. (a-c) correspond to implementation of the spin-Ising chain dynamics and (d) corresponds to a non-positive dephasing dynamics. Inset in panel (c) shows the experimentally measured distribution after the SLM implementation. **(e-h):** Phase distributions $\theta(\omega)$ of the photon frequency corresponding to (a-d).

w.r.t. increases of trace distance. In Fig. 5.7(b), coherences decay quickly and in Fig. 5.7(c), the magnitude of coherences oscillates and displays trapping. In Fig. 5.7(d), we present an example goal dynamics of non-positive dephasing whose decoherence function increases high above its initial value.

To implement the dephasing dynamics of Fig. 5.7 (a)-(d) in the polarization qubit, we use the inverse of the transformation in Eq. (5.31) to produce the distributions $|g(\omega)|^2$ and $\theta(\omega)$ which are then experimentally realized to prepare the total initial polarization–frequency state. The corresponding distributions for $|g(\omega)|^2$ are shown in Fig. 5.8 (a)-(d) and for $\theta(\omega)$ in Fig. 5.8 (e)-(h). We used $C_H = 1/\sqrt{2}$ and $C_V = \pm 1/\sqrt{2}$ as the initial values for polarization.

The experimental results for the dephasing dynamics are displayed in Fig. 5.7 (e)-(g). Comparison of the spin-Ising model dephasing dynamics of the Fig. 5.7 (a)-(c) with their experimental implementations in Fig. 5.7 (e)-(g) shows that the polarization dynamics is faithful to the dynamics of the qubit in the Ising model in all of the example cases. In addition, the correspondence between the experimental implementation and the goal dynamics of the non-positive dephasing is nearly perfect.

Chapter 6

Dynamics of Correlations

Now, we concentrate on how local noises on qubits influence the total two-qubit state from the point-of-view of correlations between the sender and recipient of a message or between the qubits. First, we study the effects of local dephasing noises on the transmission efficiency of the superdense coding protocol. We compare the behavior of mutual information between the sender and recipient with two definitions of non-Markovianity and find optimal noise configurations. Then, we find the families of initial states for whom the decay of entanglement or non-locality depends or does not depend on the location of the noise.

6.1 Memory Effects of Two-qubit Dephasing in Superdense Coding

In this section, we study memory effects in terms of revivals of trace distance and channel capacities. We consider a two-qubit system AB whose qubits experience independent and uncorrelated dephasing dynamics, meaning

$$\Phi_t^{AB} = \Phi_t^A \otimes \Phi_t^B \,, \tag{6.1}$$

where Φ_t^A and Φ_t^B are pure dephasing dynamical maps as in Eq. (5.28) for qubits A and B, respectively. We denote the local decoherence functions in Φ_t^A and Φ_t^B with $\kappa^A(t)$ and $\kappa^B(t)$. Before, we saw how the basic interpretations of memory effect based definitions of non-Markovianity differ. In this more specific case, we aim to further compare the properties of two definitions of non-Markovianity.

For a practical example of the influence of environment-induced noise,

we consider a well-known quantum communication protocol. We implement the local dephasing dynamics in the qubits used in so-called superdense coding. In this situation, multiple questions arise: How the revivals of transmission efficiency compare with the two memory effects? What should be done to maximize the information back-flow in terms of mutual information between the sender and the recipient? What can we do to maximize the transmission efficiency under local dephasing noises?

6.1.1 Memory effects

For pairs of factorized initial states of the form, $\rho_1^A(0)\otimes\rho_1^B(0)$, $\rho_2^A(0)\otimes\rho_1^B(0)$, trace distance of the evolved bipartite states simplifies to

$$D\left(\rho_1^A(t)\otimes\rho_1^B(t),\rho_2^A(t)\otimes\rho_1^B(t)\right)=D\left(\rho_1^A(t),\rho_2^A(t)\right). \tag{6.2}$$

Thus, for this kind of pairs of initial states, trace distance is sensitive only to what happens on Alice's side. Let the initial states be

$$\rho_1^{AB}=\frac{1}{2}\begin{pmatrix}1&1\\1&1\end{pmatrix}\otimes\rho^B,\quad \rho_2^{AB}=\frac{1}{2}\begin{pmatrix}1&-1\\-1&1\end{pmatrix}\otimes\rho^B. \tag{6.3}$$

For this choice, the trace distance becomes

$$D\left(\rho_1^{AB}(t),\rho_2^{AB}(t)\right)=|\kappa^A(t)|. \tag{6.4}$$

Since the BLP measure of non-Markovianity is defined as a maximization over all initial state pairs, this particular choice gives a lower bound for the BLP measure of Φ_t^{AB}. Oscillations of $|\kappa^A(t)|$ mean revivals of trace distance, and thus, non-Markovian dynamics w.r.t. BLP measure. By swapping the qubits in Eq. (6.3), the same holds for oscillations of $|\kappa^B(t)|$ which means that the revivals of either of the local decoherence functions is always detected by the BLP measure.

We solve the entanglement assisted channel capacity for the dynamical maps in Eq. (6.1) to be

$$C_{ea}(\Phi_t^{AB})=4-h_2\left[\frac{1+|\kappa^A(t)|}{2}\right]-h_2\left[\frac{1+|\kappa^B(t)|}{2}\right]. \tag{6.5}$$

Since one-qubit pure dephasing channels are degradable, we can use Eq. (3.27) and solve the quantum channel capacity for dynamical maps of Eq. (6.1). Now we get

$$Q(\Phi_t^{AB}) = 2 - h_2\left[\frac{1+|\kappa^A(t)|}{2}\right] - h_2\left[\frac{1+|\kappa^B(t)|}{2}\right], \tag{6.6}$$

so we see that the bipartite quantum channel capacity is additive, $Q(\Phi_t^{AB}) = Q(\Phi_t^A) + Q(\Phi_t^B)$. We note also that $Q(\Phi_t^{AB}) = C_{ea}(\Phi_t^{AB}) - 2$, so the entanglement assisted channel capacity and quantum capacity have revivals always at the same times.

The additivity property in Eq. (6.5) and (6.6) tells directly that combination of any two local Markovian dephasing channels always leads to a Markovian global channel. It also implies that using identical non-Markovian dephasing channels on both Alice's and Bob's side always leads to a global non-Markovian channel. However, we can also combine a Markovian and a non-Markovian channel to get either Markovian or non-Markovian global channels, depending on the local dynamical maps. We note that combining two different non-Markovian local maps may lead to Markovian global channel in sense of the BCM measure.

These results show that the BLP measure is sensitive to oscillations of the local decoherence functions. Contrary to this, the BCM measures quantify more global memory effects in the dephasing dynamics, always taking into account both local dynamics.

6.1.2 Two-qubit dephasing in superdense coding

In superdense coding, Alice and Bob initially share a pair of particles in one of the Bell states. Alice applies a unitary transformation to her qubit to change the overall state to any of the four Bell states. Subsequently, she sends her qubit to Bob, who performs a measurement to find out the overall state. Since the Bell states are orthogonal, they can be distinguished perfectly and thus four different symbols can be sent from Alice to Bob with perfect fidelity by transmitting a single qubit. This is the information capacity of two classical bits with only one qubit and one bit of entanglement [24].

Suppose Alice and Bob initially share a pair of polarization entangled photons in the Bell state $|\Phi^+\rangle$, which they use in superdense coding. In

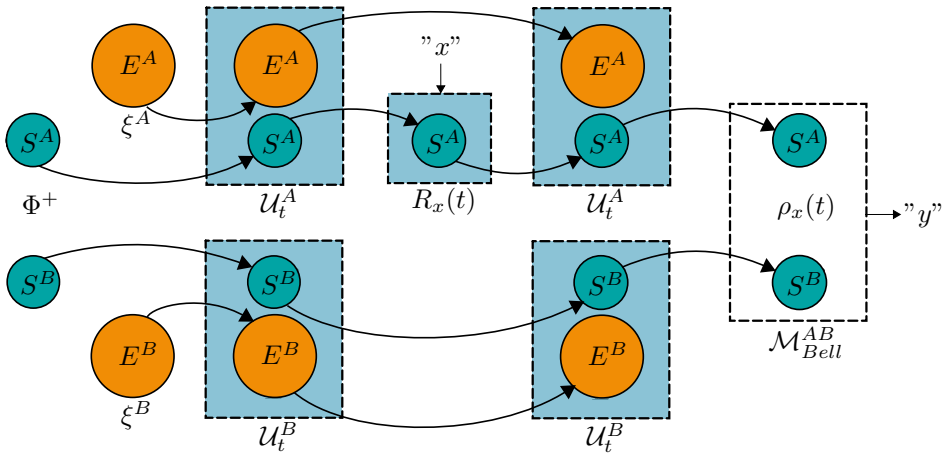

Figure 6.1: The superdense coding scheme with local dephasing noises on Alice's and Bob's qubits. Initially, Alice and Bob share a two-qubit system S^{AB} in the Bell state Φ^+. Alice's and Bob's qubits S^A and S^B interact with their local environments E^A and E^B for time $t/2$. Then, Alice encodes the symbol x by performing the unitary $R_x(t)$ on her qubit. The qubits S^A and S^B interact again with the same environments E^A and E^B for time $t/2$. Bob obtains the total two-qubit system S^{AB} in the state $\rho_x(t)$ and performs a Bell state measurement to extract the symbol y.

addition to the encoding operation on Alice's side, both photons experience local, independent dephasing dynamics caused by unitary coupling between the polarization and frequency degrees of freedom. The frequency state is characterized by the distribution $g^A(\omega^A)g^B(\omega^B)$ which is normalized so that $\int |g^j(\omega^j)|^2 d\omega^j = 1$ for $j \in \{A, B\}$. The state of the total system is

$$|\Phi^+\rangle|\xi\rangle = \frac{1}{\sqrt{2}}(|HH\rangle + |VV\rangle) \int g^A(\omega^A)g^B(\omega^B)|\omega^A\omega^B\rangle d\omega^A d\omega^B \,, \qquad (6.7)$$

and the couplings to local environments are given by the same Hamiltonian as in Eq. (5.30).

The channel structure is illustrated in Fig. 6.1. First, local polarization–frequency couplings $U^A(t/2)$ and $U^B(t/2)$ act on Alice's and Bob's photons, respectively. Then, Alice encodes the symbol x by performing a local uni-

Table 6.1: Alice's encoding unitaries and Bob's measurement outcomes corresponding to the encoded and decoded symbols, respectively.

Input x	Alice's encoding	Bob's outcome	Output y
0	$R_0(t)$	$\|\Phi^+\rangle$	0
1	$R_1(t)$	$\|\Psi^+\rangle$	1
2	$R_2(t)$	$\|\Psi^-\rangle$	2
3	$R_3(t)$	$\|\Phi^-\rangle$	3

tary $R_x(t)$ on her photon. Each unitary $R_x(t)$ is a modified Pauli operator, used to compensate for the complex phase of the decoherence functions. We choose the encoding operators $R_x(t)$ of the four possible symbols as

$$\begin{aligned} R_0(t) &= \alpha^*(t)\beta^*(t)|H\rangle\langle H| + \alpha(t)\beta(t)|V\rangle\langle V|, \\ R_1(t) &= \beta^*(t)|H\rangle\langle V| + \beta(t)|V\rangle\langle H|, \\ R_2(t) &= -i\beta^*(t)|H\rangle\langle V| + i\beta(t)|V\rangle\langle H|, \\ R_3(t) &= \alpha^*(t)\beta^*(t)|H\rangle\langle H| - \alpha(t)\beta(t)|V\rangle\langle V|. \end{aligned} \tag{6.8}$$

Here, $\alpha(t)$ and $\beta(t)$ are time dependent complex functions satisfying $|\alpha(t)| = |\beta(t)| = 1\ \forall t$. Applying each $R_x(t)$ to the initial system state $|\Phi^+\rangle$ creates four orthogonal states. The different symbols and corresponding measurements are listed in Table 6.1.

After Alice's encoding, local polarization–frequency couplings $U^A(t/2)$ and $U^B(t/2)$ act on Alice's and Bob's qubit, respectively. For a given encoding operator $R_x(t)$, the total change of the closed system is given by

$$U_x = U^A(t/2)R_x(t)U^A(t/2) \otimes U^B(t/2)U^B(t/2). \tag{6.9}$$

For different encoding operations, the reduced polarization state becomes

$$
\begin{aligned}
\rho_0(t) &= \frac{1}{2}(|HH\rangle\langle HH| + \alpha^*(t)^2\beta^*(t)^2\kappa^A(t)\kappa^B(t)|HH\rangle\langle VV| \\
&\quad + \alpha(t)^2\beta(t)^2(\kappa^A(t)\kappa^B(t))^*|VV\rangle\langle HH| + |VV\rangle\langle VV|), \\
\rho_1(t) &= \frac{1}{2}(|HV\rangle\langle HV| + \beta^*(t)^2\kappa^B(t)|HV\rangle\langle VH| \\
&\quad + \beta(t)^2(\kappa^B(t))^*|VH\rangle\langle HV| + |VH\rangle\langle VH|), \\
\rho_2(t) &= \frac{1}{2}(|HV\rangle\langle HV| - \beta^*(t)^2\kappa^B(t)|HV\rangle\langle VH| \\
&\quad - \beta(t)^2(\kappa^B(t))^*|VH\rangle\langle HV| + |VH\rangle\langle VH|), \\
\rho_3(t) &= \frac{1}{2}(|HH\rangle\langle HH| - \alpha^*(t)^2\beta^*(t)^2\kappa^A(t)\kappa^B(t)|HH\rangle\langle VV| \\
&\quad - \alpha(t)^2\beta(t)^2(\kappa^A(t)\kappa^B(t))^*|VV\rangle\langle HH| + |VV\rangle\langle VV|),
\end{aligned}
\tag{6.10}
$$

where ρ_x means that R_x was used in encoding and

$$
\begin{aligned}
\kappa^A(t) &= \int e^{i2\pi\Delta n\omega^A t}|g^A(\omega^A)|^2\mathrm{d}\omega^A\,, \\
\kappa^B(t) &= \int e^{i2\pi\Delta n\omega^B t}|g^B(\omega^B)|^2\mathrm{d}\omega^B\,,
\end{aligned}
\tag{6.11}
$$

as before.

Since mutual information quantifies correlations between two random variables X and Y, it is a natural measure of success in a situation where Alice wants to send a message formed of symbols $x \in X$ to Bob who receives a sequence of symbols $y \in Y$. For simplicity, we assume here a uniform distribution for Alice's symbols, meaning $p_A(x) = p_B(y) = \frac{1}{4}$. By using the reduced density matrices $\rho_x(t)$, corresponding to encoded symbols $x \in \{0, 1, 2, 3\}$, we calculate the mutual information to be

$$
\begin{aligned}
I(X:Y) &= \sum_{x=0}^{3}\frac{1}{4}\sum_{y=0}^{3}p(y|x)\log_2\frac{p(y|x)}{1/4} \\
&= 2 - \frac{1}{2}\left\{h_2\left[\frac{1+|\kappa^A(t)\kappa^B(t)|}{2}\right] + h_2\left[\frac{1+|\kappa^B(t)|}{2}\right]\right\}.
\end{aligned}
\tag{6.12}
$$

The form of mutual information is similar to the channel capacities in Eq. (6.5) and (6.6): the presence or absence of revivals of neither measure

can be deduced directly from the local dynamics. If both $|\kappa^A(t)\kappa^B(t)|$ and $|\kappa^B(t)|$ are monotonic, so is the mutual information. On the other hand if $|\kappa^A(t)\kappa^B(t)|$ and $|\kappa^B(t)|$ have simultaneous revivals, also the mutual information increases at those times. Unlike the BLP measure of non-Markovianity, mutual information takes both local noises into account, as expected, since both qubits are needed for superdense coding.

Let us consider a situation when there is no noise on Bob's qubit and the duration of Alice's noise before and after encoding is equal. Now, $|\kappa^B(t)| = 1$ and Eq. (6.10) shows how the states $\rho_1(t)$ and $\rho_2(t)$ are fully recovered by implementing the latter noise on qubit A. The states $\rho_0(t)$ and $\rho_3(t)$ still dephase, as they depend on $|\kappa^A(t)|$. Equation (6.12) shows that even in the worst case when $|\kappa^A(t)| = 0$, this would mean that the mutual information never decreases below 1.5. On the other hand, if Alice's qubit is affected by the noise only before encoding, $|\kappa^A(t)| = 0$ makes $\rho_0(t)$ indistinguishable from $\rho_3(t)$, and $\rho_1(t)$ indistinguishable from $\rho_2(t)$. Still, the pair $\{\rho_0(t), \rho_3(t)\}$ remains fully distinguishable from the pair $\{\rho_1(t), \rho_2(t)\}$, and thus $I(X : Y) = 1$. Comparison between these two situations shows that adding the second noise can lead up to 50 percent increase in transmission efficiency in terms of mutual information.

Unlike the quantum channel capacity, mutual information is not symmetric w.r.t. the local dehasing noises. This is a consequence of the asymmetric roles of the sender and the recipient in the superdense coding protocol. We note that swapping the initial states of the local frequency environments has immediate effect in the mutual information: Let $\kappa_1(t)$ and $\kappa_2(t)$ be two decoherence functions such that $|\kappa_1(t)| < |\kappa_2(t)|$ at some fixed interaction time t. In the mutual information, both decoherence functions appear in the first binary enropy, but only Bob's noise appears in the latter one. Thus, swapping the local noises makes no difference for the first binary entropy, so maximizing the second one maximizes $I(X : Y)$. Since $h_2[p]$ is monotonically decreasing when $p \in \left[\frac{1}{2}, 1\right]$, choosing $\kappa^A(t) = \kappa_2(t)$ and $\kappa^B(t) = \kappa_1(t)$ leads to higher mutual information than choosing the opposite. Interestingly, this means that applying noise on Bob's ancillary qubit is more harmful for superdense coding than the same noise on Alice's qubit which the encoding unitary is applied to. Similarly, if one wants to maximize the non-Markovian oscillations in mutual information, the decoherence function with more intense oscillations should be affecting Bob's qubit.

6.2 Asymmetry of correlation decay for X states

In the previous section we saw how swapping the locations of local noises has significant effect on the mutual information between the sent and received messages in superdense coding. There, the initial state was symmetric but asymmetry between the roles of Alice and Bob in the protocol led to different effects for their local noises. Now, we take a complementary approach to the symmetry of roles of the local noises: we characterize the symmetric and asymmetric initial two-qubit states leading to symmetric and asymmetric decay of quantum correlations. We consider entanglement in terms of concurrence and non-locality in terms of the CHSH Bell function.

We concentrate on a subfamily of two-qubit states known as *X states*. The family of X states is all states X, whose matrix representation w.r.t. the basis $\mathcal{B} := \{|00\rangle, |01\rangle, |10\rangle, |11\rangle\}$ is of the form

$$X = \begin{pmatrix} \rho_{11} & 0 & 0 & \rho_{14} \\ 0 & \rho_{22} & \rho_{23} & 0 \\ 0 & \rho_{23}^* & \rho_{33} & 0 \\ \rho_{14}^* & 0 & 0 & \rho_{44} \end{pmatrix} . \tag{6.13}$$

In the vector notation of basis $\mathcal{B}$, we label the first qubit as U and the latter one as L corresponding to the upper and lower qubit in Fig. 6.2, respectively.

We say, that *a state is swap symmetric* if the corresponding density matrix is invariant under swapping the qubits according to the rule $|ij\rangle \to |ji\rangle$ for $i, j \in \{0, 1\}$. An X state X in Eq. (6.13) is symmetric if and only if

$$\rho_{22} = \rho_{33} \ \wedge \ \rho_{23} \in \mathbb{R} . \tag{6.14}$$

The conditions in Eq. (6.14) are satisfied for instance by all elements of two important subclasses of X states, namely Bell-diagonal and Werner states.

We concentrate on one-sided channels, which means that the channel influences only one of the local qubit states at a time as in Fig. 6.2. We

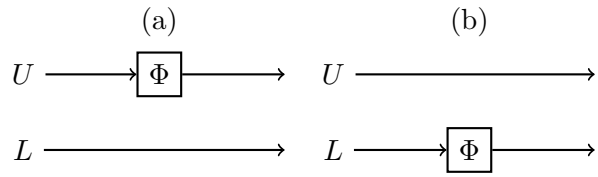

Figure 6.2: The different noise configurations. Alice sends a two-qubit system to Bob. Qubits U and L are transmitted through the upper and lower path, respectively. In (a) and (b) the local noise influences the qubit U and L, respectively.

denote the one-sided channels affecting qubits U and L by

$$\Phi^U(\rho) := \sum_i (K_i' \otimes \mathbb{1}^L)\rho(K_i'^\dagger \otimes \mathbb{1}^L)\,, \tag{6.15}$$

$$\Phi^L(\rho) := \sum_i (\mathbb{1}^U \otimes K_i')\rho(\mathbb{1}^U \otimes K_i'^\dagger)\,, \tag{6.16}$$

respectively. We say that *the dynamics of a state ρ is symmetric* if $\Phi^U(\rho) = \Phi^L(\rho)$. For pure dephasing channel, given by Kraus operators $\sqrt{1-p}\mathbb{1}$, and $\sqrt{p}\sigma_3$, we notice that $\Phi_p^U(X) = \Phi_p^L(X)$ for all initial X states X. Thus all the properties of the system, such as entanglement and Bell function evolve symmetrically with respect to the location of the noise.

Next we study the conditions leading to symmetric and asymmetric state dynamics, entanglement decay, and decay of non-locality under the effects of depolarizing and amplitude damping channels.

6.2.1 Asymmetry in entanglement decay

It has been shown that, for all X states, concurrence can be obtained directly from the matrix elements as [112]:

$$C(X) = 2\max\left\{0,\, |\rho_{23}| - \sqrt{\rho_{11}\rho_{44}},\, |\rho_{14}| - \sqrt{\rho_{22}\rho_{33}}\right\}. \tag{6.17}$$

One set of Kraus operators for depolarizing channel are $K_1' = \frac{\sqrt{p}}{2}\sigma_1$, $K_2' = \frac{\sqrt{p}}{2}\sigma_2$, $K_3' = \frac{\sqrt{p}}{2}\sigma_3$, and $K_4' = \sqrt{1-\frac{3p}{4}}\mathbb{1}$. Here, the parameter $p \in [0,1]$ quantifies the strength of the channel: if $p = 0$, the state is not changed

at all and if $p = 1$, the channel influences the state as much as it is allowed. By comparing $\Phi_p^U(X)$ and $\Phi_p^L(X)$ for depolarizing channel Φ_p with strength parameter p, it is evident, that the dynamics of a state is symmetric if and only if $\rho_{11} = \rho_{44}$ and $\rho_{22} = \rho_{33}$. We note that the symmetry of the state dynamics is independent of the phase of ρ_{23}, unlike the symmetry of the initial state, but it requires $\rho_{11} = \rho_{44}$ instead. By using Eq. (6.17) we get the concurrences of the output states as

$$\begin{aligned} C\big(\Phi_p^U(X)\big) = 2\max\Big\{0, q|\rho_{23}| - \frac{1}{2}\sqrt{(2\rho_{11}+r_{31}p)(2\rho_{44}+r_{24}p)}, \\ q|\rho_{14}| - \frac{1}{2}\sqrt{(2\rho_{33}+r_{13}p)(2\rho_{22}+r_{42}p)}\Big\}, \\ C\big(\Phi_p^L(X)\big) = 2\max\Big\{0, q|\rho_{23}| - \frac{1}{2}\sqrt{(2\rho_{11}+r_{21}p)(2\rho_{44}+r_{34}p)}, \\ q|\rho_{14}| - \frac{1}{2}\sqrt{(2\rho_{22}+r_{12}p)(2\rho_{33}+r_{43}p)}\Big\}, \end{aligned} \tag{6.18}$$

where we have denoted

$$r_{jk} := \rho_{jj} - \rho_{kk}, \quad q := 1 - p\,. \tag{6.19}$$

Entanglement decays symmetrically, i.e. $C\big(\Phi_p^U(X)\big) = C\big(\Phi_p^L(X)\big)\,\forall p \in [0,1]$, if and only if $\rho_{33} = \rho_{22}$ or $\rho_{11} = \rho_{44}$. The first condition is necessary for the symmetry of the initial state, as formulated in Eq. (6.14). Instead the second one, $\rho_{11} = \rho_{44}$, is not. So, the symmetry of entanglement decay requires neither swap symmetry of the initial state nor symmetry in the dynamics of the state.

For amplitude damping channels, the Kraus operators can be chosen as $K_1' = \frac{\sqrt{p}}{2}\sigma_+$, and $K_2' = \frac{1+\sqrt{1-p}}{2}\mathbb{1} + \frac{1-\sqrt{1-p}}{2}\sigma_3$. Comparison of $\Phi_p^U(X)$ and $\Phi_p^L(X)$ for amplitude damping channel Φ_p shows, that the dynamics of a state is symmetric if and only if $X = |11\rangle\langle 11|$, which is invariant. This means that the amplitude damping dynamics is symmetric only for one initial state which is swap symmetric, unlike in the case of depolarizing

channel. By (6.17), we get the concurrences of the output states as

$$\begin{aligned} C(\Phi_p^U(X)) &= 2\max\Big\{0,\sqrt{q}\Big(|\rho_{23}| - \sqrt{\rho_{44}(\rho_{11}+\rho_{33}p)}\Big), \\ &\qquad \sqrt{q}\Big(|\rho_{14}| - \sqrt{\rho_{33}(\rho_{22}+\rho_{44}p)}\Big)\Big\}, \\ C(\Phi_p^L(X)) &= 2\max\Big\{0,\sqrt{q}\Big(|\rho_{23}| - \sqrt{\rho_{44}(\rho_{11}+\rho_{22}p)}\Big), \\ &\qquad \sqrt{q}\Big(|\rho_{14}| - \sqrt{\rho_{22}(\rho_{33}+\rho_{44}p)}\Big)\Big\}. \end{aligned} \tag{6.20}$$

Now entanglement decay is symmetric if and only if $\rho_{33} = \rho_{22}$ or $\rho_{44} = 0$. The first condition is necessary for the symmetry of the initial state but the second one, $\rho_{44} = 0$, is not related to it. So again, an initially asymmetric state can lead to symmetric decay of entanglement. Also, initial states leading to asymmetric state dynamics can have symmetric decay for entanglement.

6.2.2 Asymmetry in decay of non-locality

For X states, the Bell function $\mathfrak{B}_{CHSH}$ in Eq. (3.36) becomes

$$\begin{aligned} &\mathfrak{B}^j_{CHSH} = 2\sqrt{u_1^j + \max\{u_2^j,\, u_3^j\}}\,, \quad \text{where} \\ &u_1^j = 4(|\rho_{14}| + |\rho_{23}|)^2\,,\ u_2^j = (r_{12}+r_{43})^2\,,\ u_3^j = 4(|\rho_{14}| - |\rho_{23}|)^2\,, \end{aligned} \tag{6.21}$$

and the superscript $j \in \{U, L\}$ corresponds to the noise location. For short, we denote $\mathfrak{B}^j_{CHSH,1} = 2\sqrt{u_1^j + u_2^j}$ and $\mathfrak{B}^j_{CHSH,2} = 2\sqrt{u_1^j + u_3^j}$.

Next we study the behavior of $\mathfrak{B}_{CHSH}$ under local depolarizing and amplitude damping channels and their combinations. As in the case of entanglement, also here we are interested in whether the dynamics of $\mathfrak{B}_{CHSH}$ depends on the location of the noise.

For one-sided depolarizing channel, we see that

$$\begin{aligned} \mathfrak{B}^U_{CHSH,1} &= \mathfrak{B}^L_{CHSH,1} = 2q\sqrt{4(\rho_{14}+\rho_{23})^2 + (r_{12}+r_{43})^2}\,, \\ \mathfrak{B}^U_{CHSH,2} &= \mathfrak{B}^L_{CHSH,2} = 4q\sqrt{2(|\rho_{14}|^2 + |\rho_{23}|^2)}\,. \end{aligned} \tag{6.22}$$

This means that the effect of depolarizing noise on non-locality of the state is independent of the location for all X states. Since certain initial states lead to asymmetric entanglement decay in depolarizing channel, this implies

Table 6.2: Behavior of entanglement decay (ED) and decay of non-locality (ND) for different families of initial states.

(a) *Depolarizing channel.*

	$\rho_{22} = \rho_{33}$	$\rho_{22} \neq \rho_{33} \wedge$ $\rho_{11} = \rho_{44} \neq 0$	$\rho_{22} \neq \rho_{33} \wedge$ $\rho_{11} = \rho_{44} = 0$	$\rho_{22} \neq \rho_{33} \wedge$ $\rho_{11} \neq \rho_{44} = 0$
ED	Symmetric	Symmetric	Symmetric	**Asymmetric**
ND	Symmetric	Symmetric	Symmetric	**Symmetric**

(b) *Amplitude damping channel.*

	$\rho_{22} = \rho_{33}$	$\rho_{22} \neq \rho_{33} \wedge$ $\rho_{11} = \rho_{44} \neq 0$	$\rho_{22} \neq \rho_{33} \wedge$ $\rho_{11} = \rho_{44} = 0$	$\rho_{22} \neq \rho_{33} \wedge$ $\rho_{11} \neq \rho_{44} = 0$
ED	Symmetric	Asymmetric	**Symmetric**	**Symmetric**
ND	Symmetric	Asymmetric	**Asymmetric**	**Asymmetric**

that non-locality and entanglement behave in different way in terms of location of the noise.

For one-sided amplitude damping channel, we see that

$$\mathfrak{B}^{U}_{CHSH,1} = 2\sqrt{4q(|\rho_{14}| + |\rho_{23}|)^2 + \left[r_{12} + (2p-1)r_{34}\right]^2}\,, \tag{6.23}$$

$$\mathfrak{B}^{U}_{CHSH,2} = \mathfrak{B}^{L}_{CHSH,2} = 4\sqrt{2q(|\rho_{14}|^2 + |\rho_{23}|^2)}\,, \tag{6.24}$$

$$\mathfrak{B}^{L}_{CHSH,1} = 2\sqrt{4q(|\rho_{14}| + |\rho_{23}|)^2 + \left[r_{13} + (2p-1)r_{24}\right]^2}\,. \tag{6.25}$$

Comparison of Eq. (6.23) and (6.25) shows that when $\mathfrak{B}_{CHSH,1} > \mathfrak{B}_{CHSH,2}$, the location of the noise makes a difference, unlike in the case of depolarizing channel. We see that $\mathfrak{B}^{U}_{CHSH,1} = \mathfrak{B}^{L}_{CHSH,1}\ \forall p \in [0,1]$ if and only if $\rho_{22} = \rho_{33}$ or $\rho_{11} = \rho_{44} = (\rho_{22} + \rho_{33})/2 = 1/4$. The first condition is satisfied by all symmetric initial states, so, as in the case of concurrence, also symmetric decay of non-locality follows always from symmetric initial state. On the other hand, the second condition does not require symmetric initial state. For all initial X states satisfying the second condition, the value of $\mathfrak{B}_{CHSH}$ is maximized with the choice $\rho_{11} = \rho_{22} = \rho_{33} = \rho_{44} = |\rho_{14}| = |\rho_{23}| = 1/4$.

For this state we get $\mathfrak{B}_{CHSH} = 2$, which is not interesting in the context of decay of non-locality, since such state is initially local.

In Table 6.2, we summarize our results concerning the symmetry conditions of entanglement and non-locality decay for depolarizing and amplitude damping dynamics. We note, that there are families of initial X states whose entanglement, or non-locality decay is symmetric or asymmetric for both channels. There are also some families for which the entanglement and non-locality have both symmetric or asymmetric decay. The most interesting family of initial states shows absolute lack of hierarchy in the symmetries of the studied correlation measures: For depolarizing dynamics, the decay of entanglement is asymmetric and the decay of Bell function is symmetric. Contrary to this, the decay of concurrence is symmetric and the decay of Bell function asymmetric for the same states in depolarizing dynamics.

Chapter 7

Conclusions

This thesis focused on quantum information-centered approaches to open quantum systems. These two fields coexist in a symbiotic relationship: As the information carrier in any realistic implementation of quantum information protocol interacts with some kind of environment, research of open quantum systems is essential to minimize the loss of information. On the other hand, quantifying information has turned out to be fruitful to the theory of open quantum systems: since memory effects can be interpreted as information back flow, they can be used to construct more physical definitions to quantum Markovianity and non-Markovianity.

In this thesis, we studied the effects of system-environment interaction in open quantum systems as well as information exchange from many different but complementary perspectives: We studied the conditions of physicality and memory effects – and how to experimentally implement non-positive dynamics, often considered non-physical. We derived restrictions in reservoir engineering – and showed how to gain full control of the dynamics. We quantified the information-destroying effect of environment-induced noise – and explained how to exploit it to gain information about the environment. We analyzed the damages caused by noise in a quantum communication protocol – and how noise can sometimes be fought by adding more noise. We showed how loss of information from quantum system prepared in a symmetric state is sensitive to the noise location in asymmetric configuration – and when the decay of correlations of asymmetric states is independent of the noise location. Some of these considerations were purely theoretical, but some could be experimentally implemented with existing technologies. In two cases, the results were experimentally tested and verified.

In Chapter 2, we started by recalling some important mathematical def-

initions and basic structures of Hilbert space quantum mechanics. We also presented some of the main results in the theory of open quantum systems concerning the dynamical maps of the system state. In Chapter 3, we discussed the required information measures and the concept of classical and quantum Markovianity, connecting open system dynamics to information in a natural way.

In Chapter 4, we summarized some results of Publications **II** and **V**, characterizing the physicality and memory effects of phase-covariant single qubit master equations. The phase covariant family contains a large variety of dynamical maps including both unital, for example pure dephasing and depolarizing dynamics, and non-unital, such as amplitude damping dynamics. We derived the explicit conditions for complete positivity in terms of the time-dependent decay rates for this complicated class of dynamical maps. We also derived the necessary and sufficient conditions for different memory effects to occur. Together, these results allow one to conclude directly from the decay rates whether the resulting dynamical map will be completely positive or not and which of the memory effects will occur without explicitly solving the dynamical map or performing the optimizations for each memory effect. Alternatively, these results give tools to construct dynamical maps which manifest exactly the desired memory effects at the wanted times and whose physicality is guaranteed.

Chapter 5 concentrated on probing measurements and reservoir engineering results of Publications **III**, **VII**, and **VI**. We started by defining the family of α-fidelities for states, which contains the commonly used fidelity function. We derived an inequality between α-fidelities of pairs of initial states of the system and environment and the α-fidelity of the evolved system states in the open quantum system picture with no initial correlations. The derived inequality was proven powerful in different applications.

First, we showed how it can be used to develop quantum probing protocols in situations where the coupling between the probe and the system of interest is completely unknown. We demonstrated how the probing works in an example case of probe qubit interacting with harmonic oscillator in thermal state with unknown frequency and tunable temperature. This example also showed that the freedom in α-parameter leads to higher accuracy in probing. We presented and experimentally implemented an informationally incomplete measurement which solves so-called membership problems w.r.t. α-fidelities. The successful experiment proved two things: First, experimentally determining the values of α-fidelity needed in our

probing protocols does not require full tomography. Secondly, it showed that multi-partite membership problems can be experimentally solved with informationally incomplete measurements by using the geometric approach of [64].

Then, we saw how the inequality of α-fidelities can be used to see what kind of restrictions the closeness of initial environment states corresponding to known and unknown dephasing dynamics set to the unknown dynamics as a function of the known decoherence function. If the fidelity between the environmental states is large enough, these restrictions can be used to guarantee characteristic properties of the unknown decoherence functions, namely occurrence of memory effects and coherence trapping. We continued with dephasing dynamics but went beyond the assumption of initially uncorrelated system and environment. We showed how precise control of the initial correlations and the state of the environment gives us full control over the dephasing dynamics of the polarization qubit and the entanglement between polarization and frequency. We demonstrated how exploiting the initial correlations lets us implement and control even non-positive dynamics. These results were experimentally realized and the measurement results were in good agreement with the theoretical predictions.

Finally, Chapter 6 presented the results of Publications **I** and **IV**, considering memory effects and dynamics of correlations in bipartite systems. We compared the memory effects in terms of trace distance and channel capacities in local and independent dephasing dynamics for two qubits. Then, we studied the effect of polarization dephasing dynamics of Chapter 5 in the mutual information of superdense coding protocol. We noted that the mutual information depended explicitly on both of the local noises in a similar way as the channel capacities. Contrary to this, the trace distance based BLP measure was sensitive to local dynamics and it could detect the non-Markovianity rising from each of the local maps separately.

We compared the effect of noises on Alice's and Bob's qubits in superdense coding. When Alice performs the unitary encoding, surprisingly the noise on Bob's qubit is more harmful to the transmission efficiency. We also concluded that if the goal is to maximize oscillations of mutual information, the more intensively oscillating local dephasing noise should be implemented on Bob's qubit. In cases where Bob's qubit does not experience any noise, and dephasing noise affects Alice's qubit only before the encoding, we notice that implementing identical noise on Alice's qubit after the encoding increases the mutual information: even in the worst case of

complete decoherence, Alice can send 1.5 bits of information in each qubit transmitted to Bob.

To complete our study of symmetric and asymmetric roles of local noises, we characterized the classes of so-called X states whose state dynamics, loss of entanglement, or decay of non-locality does or does not depend on the choice of which qubit is exposed to the the noise. We noticed that for any X state the dephasing dynamics does not depend on the location of the noise, and as a consequence, loss of the studied correlation measures is independent of the noise location. Contrary to this, the set of states leading to symmetric or asymmetric dynamics of correlations is non-trivial for depolarizing and amplitude damping channels. The most interesting family shows that there cannot exist any hierarchy between the symmetries of decay of entanglement and non-locality: Under depolarizing dynamics entanglement decays asymmetrically but non-locality has symmetric dynamics w.r.t. the noise location. On the other hand, the results are completely opposite for amplitude damping channels.

To conclude, we have studied the harmful effects of open system dynamics and how to control or exploit them in many scenarios and for different purposes. The research can be continued in many directions: Recently, the BLP non-Markovianity was linked directly to the quantum speed limit time of amplitude damping channels [113]. It is an open question, if similar connection exists to other dynamical maps or is BLP the only measure of non-Markovianity with such link. With our classification of memory effects, the connection between the quantum speed limit time and different memory effects of more general phase-covariant dynamics could be studied. In addition to our α-fidelity, other functions can be used to derive inequalities which are similar to the one we exploited in quantum probing. Thus, it is worth studying if other functions would perform better in probing or could they be easier to handle than α-fidelity. In the probing example, we chose a single qubit as our probe. Recently, quantum correlated probes have been proven to be useful in quantum estimation [114]. A natural question rises: can entangling our probe qubit with some ancillary system lead to tighter bounds for the unknown parameter?

When controlling the polarization dephasing dynamics, we acquired very precise control of the system-environment correlations and the initial environment state. This opens new possibilities to structured and controlled interference. We concentrated on dephasing w.r.t. a fixed direction. It is left to see how high control of dynamics can be achieved when the de-

phasing direction is rotated in time. The control of dephasing dynamics can be extended to multi-photon situations with initial correlations between the polarization states and frequency states of different photons. Combining this with rotated dephasing axes could result to versatile control of dynamics. Also the dynamics of correlations between different system pairs could be studied and controlled, as we did for the correlations between polarization and frequency.

Bibliography

[1] Y. Ji, Y. Chung, D. Sprinzak, M. Heiblum, D. Mahalu, and H. Shtrikman. *Nature*, 422:415–418, (2003).

[2] R. Bach, D. Pope, S.-H. Liou, and H. Batelaan. *New J. Phys.*, 15:033018, (2013).

[3] L. Maccone and A. K. Pati. *Phys. Rev. Lett.*, 113:260401, (2014).

[4] T. Heinosaari, T. Miyadera, and M. Ziman. *J. Phys. A: Mathematical and Theoretical*, 49:123001, (2016).

[5] C. H. Bennett, G. Brassard, and N. D. Mermin. *Phys. Rev. Lett.*, 68:557–559, (1992).

[6] C. A. Fuchs and A. Peres. *Phys. Rev. A*, 53:2038–2045, (1996).

[7] L. Maccone. *Phys. Rev. A*, 73:042307, (2006).

[8] T. J. Herzog, P.G. Kwiat, H. Weinfurter, and A. Zeilinger. *Phys. Rev. Lett.*, 75:3034–3037, (1995).

[9] S. P. Walborn, M. O. Terra Cunha, S. Pádua, and C. H. Monken. *Phys. Rev. A*, 65:033818, (2002).

[10] K. Kang. *Phys. Rev. B*, 75:125326, (2007).

[11] M. A. Nielsen and I. L. Chuang. *Quantum Computation and Quantum Information: 10th Anniversary Edition.* Cambridge University Press, (2011).

[12] T. Heinosaari and M. Ziman. *The Mathematical Language of Quantum Theory: From Uncertainty to Entanglement.* Cambridge University Press, (2011).

[13] C. H. Bennett., Gilles G. Brassard, C. Crépeau, R. Jozsa, A. Peres, and W. K. Wootters. *Phys. Rev. Lett.*, 70:1895–1899, (1993).

[14] E. Schrödinger. *Proc. Cambridge Philos. Soc.*, 31:555–563, (1935).

[15] C. H. Bennett, H. J. Bernstein, S. Popescu, and B. Schumacher. *Phys. Rev. A*, 53:2046–2052, (1996).

[16] W. K. Wootters. *Phys. Rev. Lett.*, 80:2245–2248, (1998).

[17] A. Einstein, B. Podolsky, and N. Rosen. *Phys. Rev.*, 47:777–780, (1935).

[18] J. F. Clauser, M. A. Horne, A. Shimony, and R. A. Holt. *Phys. Rev. Lett.*, 23:880–884, (1969).

[19] B. Hensen & al. *Nature*, 526:682–686, (2015).

[20] J. Yin & al. *Science*, 356:1140–1144, (2017).

[21] The BIG Bell Test Collaboration. *Nature*, 557:212–216, (2018).

[22] C. H. Bennett and G. Brassard. Quantum cryptography: Public key distribution and coin tossing. In *Proceedings of IEEE International Conference on Computers, Systems, and Signal Processing*, page 175, (1984).

[23] A. K. Ekert. *Phys. Rev. Lett.*, 67:661–663, (1991).

[24] C. H. Bennett and S. J. Wiesner. *Phys. Rev. Lett.*, 69:2881–2884, (1992).

[25] D. Deutsch and R. Jozsa. *Proc. R. Soc. A*, 439:553–558, (1992).

[26] P. W. Shor. Algorithms for quantum computation: discrete logarithms and factoring. In *Proceedings 35th Annual Symposium on Foundations of Computer Science*, pages 124–134, (1994).

[27] L. K. Grover. *Phys. Rev. Lett.*, 79:325–328, (1997).

[28] A. Montanaro. *npj Quantum Inf.*, 2:15023, (2016).

[29] S. Gulde, M. Riebe, G. P. T. Lancaster, C. Becher, J. Eschner, H. Häffner, F. Schmidt-Kaler, I. L. Chuang, and R. Blatt. *Nature*, 421:48–50, (2003).

[30] L. M. K. Vandersypen, M. Steffen, G. Breyta, C. S. Yannoni, M. H. Sherwood, and I. L. Chuang. *Nature*, 414:883–887, (2001).

[31] I. L. Chuang, N. Gershenfeld, and M. Kubinec. *Phys. Rev. Lett.*, 80:3408–3411, (1998).

[32] J.-G. Ren & al. *Nature*, 549:70–73, (2017).

[33] J. M. Gambetta, J. M. Chow, and M. Steffen. *npj Quantum Inf.*, 3:2, (2017).

[34] R. Harper and S. T. Flammia. *Phys. Rev. Lett.*, 122:080504, (2019).

[35] M. A Schlosshauer. *Decoherence and the Quantum-To-Classical Transition.* Springer-Verlag, (2007).

[36] D. Suter and G. A. Álvarez. *Rev. Mod. Phys.*, 88:041001, (2016).

[37] H. P. Breuer and F. Petruccione. *The theory of open quantum systems.* Oxford University Press, (2002).

[38] R. Alicki and K. Lendi. *Quantum dynamical semigroups and applications.* Springer-Verlag, (2007).

[39] Á. Rivas and S. F. Huelga. *Open Quantum Systems: An Introduction.* Springer-Verlag, (2011).

[40] I. Rotter and J. P. Bird. *Rep. Prog. Phys.*, 78:114001, (2015).

[41] C. J. Myatt, B. E. King, Q. A. Turchette, C. A. Sackett, D. Kielpinski, W. M. Itano, C. Monroe, and D. J. Wineland. *Nature*, 403:269–273, (2000).

[42] H.-P. Breuer, E.-M. Laine, and J. Piilo. *Phys. Rev. Lett.*, 103:210401, (2009).

[43] S. Lorenzo, F. Plastina, and M. Paternostro. *Phys. Rev. A*, 88:020102, (2013).

[44] B. Bylicka, D. Chruściński, and S. Maniscalco. *Scientific Reports*, 4:5720, (2014).

[45] Z. He, L. Li, C. M. Yao, and Y. Li. *Acta Physica Sinica*, 64:140302, (2015).

[46] Á. Rivas, S. F. Huelga, and M. B. Plenio. *Rep. Prog. Phys.*, 77:094001, (2014).

[47] H.-P. Breuer, E.-M. Laine, J. Piilo, and B. Vacchini. *Rev. Mod. Phys.*, 88:021002, (2016).

[48] I. de Vega and D. Alonso. *Rev. Mod. Phys.*, 89:015001, (2017).

[49] L. Li, M. J. W. Hall, and H. M. Wiseman. *Physics Reports*, 759:1 – 51, (2018).

[50] C. Addis, B. Bylicka, D. Chruściński, and S. Maniscalco. *Phys. Rev. A*, 90:052103, (2014).

[51] B.-H. Liu, X.-M. Hu, Y.-F. Huang, C.-F. Li, G.-C. Guo, A. Karlsson, E.-M. Laine, S. Maniscalco, C. Macchiavello, and J. Piilo. *EPL*, 114:10005, (2016).

[52] Y. Dong, Y. Zheng, S. Li, C.-C. Li, X.-D. Chen, G.-C. Guo, and F.-W. Sun. *npj Quantum Inf.*, 4:3, (2018).

[53] M. A. Nielsen and I. L. Chuang. *Phys. Rev. Lett.*, 79:321–324, (1997).

[54] J. I. Cirac and P. Zoller. *Nature Physics*, 8:264–266, (2012).

[55] J. T. Barreiro, M. Müller, P. Schindler, D. Nigg, T. Monz, M. Chwalla, M. Hennrich, C. F. Roos, P. Zoller, and R. Blatt. *Nature*, 470:486–491, (2011).

[56] S. Cialdi, M. A. C. Rossi, C. Benedetti, B. Vacchini, D. Tamascelli, S. Olivares, and M. G. A. Paris. *Appl. Phys. Lett.*, 110:081107, (2017).

[57] Á. Cuevas, A. Geraldi, C. Liorni, L. D. Bonavena, A. De Pasquale, F. Sciarrino, V. Giovannett, and P. Mataloni. *Scientific Reports*, 9:3205, (2019).

[58] M. Bruderer and D. Jaksch. *New J. Phys.*, 8:87–87, (2006).

[59] C. Guerlin, J. Bernu, S. Deléglise, C. Sayrin, S. Gleyzes, S. Kuhr, M. Brune, J.-M. Raimond, and S. Haroche. *Nature*, 448:889–893, (2007).

[60] P. Haikka, S. McEndoo, and S. Maniscalco. *Phys. Rev. A*, 87:012127, (2013).

[61] R. Dorner, S. R. Clark, L. Heaney, R. Fazio, J. Goold, and V. Vedral. *Phys. Rev. Lett.*, 110:230601, (2013).

[62] D. Tamascelli, C. Benedetti, S. Olivares, and M. G. A. Paris. *Phys. Rev. A*, 94:042129, (2016).

[63] A. Abdelrahman, O. Khosravani, M. Gessner, A. Buchleitner, H.-P. Breuer, D. Gorman, R. Masuda, T. Pruttivarasin, M. Ramm, P. Schindler, and H. Häffner. *Nat. Commun.*, 8:15712, (2017).

[64] C. Carmeli, T. Heinosaari, A. Karlsson, J. Schultz, and A. Toigo. *Phys. Rev. Lett.*, 116:230403, (2016).

[65] B.-H. Liu, L. Li, Y.-F. Huang, C.-F. Li, G.-C. Guo, E.-M. Laine, H.-P. Breuer, and J. Piilo. *Nature Physics*, 7:931–934, (2011).

[66] P. Pechukas. *Phys. Rev. Lett.*, 73:1060–1062, (1994).

[67] E.-M. Laine, J. Piilo, and H.-P. Breuer. *EPL*, 92:60010, (2010).

[68] P. Busch, M. Grabowski, and P. J. Lahti. *Operational Quantum Physics*. Springer-Verlag, (2013).

[69] P. Busch, P. J. Lahti, J.-P. Pellonpää, and K. Ylinen. *Quantum Measurement*. Springer International, (2016).

[70] G. M. D'Ariano, G. Chiribella, and P. Perinotti. *Quantum Theory from First Principles: An Informational Approach*. Cambridge University Press, (2017).

[71] M. D. Choi. *Linear Algebra Appl.*, 10:285–290, (1975).

[72] A. S. Holevo and V. Giovannetti. *Rep. Prog. Phys.*, 75:046001, (2012).

[73] V. Gorini, A. Kossakowski, and E. C. G. Sudarshan. *J. Math. Phys.*, 17:821–825, (1976).

[74] G. Lindblad. *Commun. Math. Phys.*, 48:119, (1976).

[75] C. W. Helstrom. *Quantum Detection and Estimation Theory.* Academic, (1976).

[76] A. Gilchrist, N.K. Langford, and M. A. Nielsen. *Phys. Rev. A*, 71:062310, (2005).

[77] M. J. W. Hall, J.D. Cresser, L. Li, and E. Andersson. *Phys. Rev. A*, 89:042120, (2014).

[78] B. Schumacher. *Phys. Rev. A*, 51:2738–2747, (1995).

[79] A. Uhlmann. *Reports on Mathematical Physics*, 9:273 – 279, (1976).

[80] R. Jozsa. *Journal of Modern Optics*, 41:2315–2323, (1994).

[81] I. L. Chuang, L. M. K. Vandersypen, X. Zhou, D. W. Leung, and S. Lloyd. *Nature*, 393:143, (1998).

[82] N. A. Gershenfeld and I. L. Chuang. *Science*, 275:350–356, (1997).

[83] J. Joo, W. J. Munro, and T. P. Spiller. *Phys. Rev. Lett.*, 107:083601, (2011).

[84] N. Lambert, Y.-N. Chen, Y.-C. Cheng, C.-M. Li, G.-Y. Chen, and F. Nori. *Nature Physics*, 9:10, (2013).

[85] T. Baumgratz, M. Cramer, and M. B. Plenio. *Phys. Rev. Lett.*, 113:140401, (2014).

[86] D. Girolami. *Phys. Rev. Lett.*, 113:170401, (2014).

[87] J. Svozilík, A. Vallés, J. Peřina, and J. P. Torres. *Phys. Rev. Lett.*, 115:220501, (2015).

[88] C. E. Shannon. *Bell system technical journal*, 27, (1948).

[89] P. W. Shor. *Phys. Rev. A*, 52:R2493–R2496, (1995).

[90] A. M. Steane. *Phys. Rev. Lett.*, 77:793–797, (1996).

[91] R. Raussendorf. *Philos. Trans. Royal Soc. A: Mathematical, Physical and Engineering Sciences*, 370:4541–4565, (2012).

[92] E. T. Campbell, B. M. Terhal, and C. Vuillot. *Nature*, 549:172–179, (2017).

[93] B.-H. Liu, D.-Y. Cao, Y.-F. Huang, C.-F. Li, G.-C. Guo, E.-M. Laine, H.-P. Breuer, and J. Piilo. *Scientific Reports*, 3:21–33, (2013).

[94] B.-H. Liu, L. Li, Y.-F. Huang, C.-F. Li, G.-C. Guo, E.-M. Laine, H.-P. Breuer, and J. Piilo. *Nature Physics*, 7:931–934, (2011).

[95] B. Schumacher and M. A. Nielsen. *Phys. Rev. A*, 54:2629–2635, (1996).

[96] M. M. Wilde. *Quantum Information Theory*. Cambridge University Press, (2013).

[97] I. Devetak and P. W. Shor. *Commun. Math. Phys*, 256:287–303, (2005).

[98] R. Horodecki, P. Horodecki, and M. Horodecki. *Physics Letters A*, 200:340 – 344, (1995).

[99] Á. Rivas, S. F. Huelga, and M. B. Plenio. *Rep. Prog. Phys.*, 77:094001, (2014).

[100] A. Smirne, J. Kołodyński, S. F. Huelga, and R. Demkowicz-Dobrzański. *Phys. Rev. Lett.*, 116:120801, (2016).

[101] A. Fujiwara and P. Algoet. *Phys. Rev. A*, 59:3290–3294, (1999).

[102] M. B. Ruskai, S. Szarek, and E. Werner. *Linear Algebra Its Appl.*, 347:159 – 187, (2002).

[103] M. Müller-Lennert, F. Dupuis, O. Szehr, S. Fehr, and M. Tomamichel. *J. Math. Phys.*, 54:122203, (2013).

[104] M. M. Wilde, A. Winter, and D. Yang. *Commun. Math. Phys.*, 331:593–622, (2014).

[105] H. T. Quan, Z. Song, X. F. Liu, P. Zanardi, and C. P. Sun. *Phys. Rev. Lett.*, 96:140604, (2006).

[106] P. Haikka, J. Goold, S. McEndoo, F. Plastina, and S. Maniscalco. *Phys. Rev. A*, 85:060101, (2012).

[107] C. Carmeli, T. Heinosaari, J. Schultz, and A. Toigo. *Proc. R. Soc. A*, 473:20160866, (2017).

[108] D. Lu, T. Xin, N. Yu, Z. Ji, J. Chen, G. Long, J. Baugh, X. Peng, B. Zeng, and R. Laflamme. *Phys. Rev. Lett.*, 116:230501, (2016).

[109] R. A. Bertlmann and P. Krammer. *J. Phys. A: Mathematical and Theoretical*, 41:235303, (2008).

[110] E.-M. Laine, H.-P. Breuer, J. Piilo, C.-F. Li, and G.-C. Guo. *Phys. Rev. Lett.*, 108:210402, (2012).

[111] A. Karlsson, H. Lyyra, E.-M. Laine, S. Maniscalco, and J. Piilo. *Phys. Rev. A*, 93:032135, (2016).

[112] T. Yu and J. H. Eberly. *Quantum Info. Comput.*, 7:459–468, (2007).

[113] Z.-Y. Xu, S. Luo, W. L. Yang, C. Liu, and S. Zhu. *Phys. Rev. A*, 89:012307, (2014).

[114] D. Girolami, A. M. Souza, V. Giovannetti, T. Tufarelli, J. G. Filgueiras, R. S. Sarthour, D. O. Soares-Pinto, I. S. Oliveira, and G. Adesso. *Phys. Rev. Lett.*, 112:210401, (2014).

UNIVERSITY
OF TURKU

ISBN 978-951-29-7762-8 (PRINT)
ISBN 978-951-29-7763-5 (PDF)
ISSN 0082-7002 (PRINT) ISSN 2343-3175 (ONLINE)

Painosalama Oy, Turku , Finland 2019